p-^{3}He Effective Potentials based on the Pauli Corrected Resonating Group Method

S. Gojuki [1], S. Oryu[1*], and S. A. Sofianos[2]
[1] *Department of Physics, Faculty of Science and Technology, Science University of Tokyo, 2641 Yamazaki, Noda, Chiba 278-8510, Japan*
[2] *Physics Department, University of South Africa, Pretoria 0003, South Africa*
(December 10, 2001)

Abstract

Effective interactions that fit the low energy p-^{3}He experimental data have been constructed. They are based on the Resonating Group Method and a modified Orthogonality Condition Model in which Pauli and partly Pauli forbidden states are removed from the spectrum. Partial waves up to $L = 3$ have been considered. The LS force acting between the proton and ^{3}He has been included phenomenologically, while the Coulomb interaction has been incorporated using a renormalization technique for a screened Coulomb interaction. The potentials are also given in a separable momentum space form, obtained using the Ernst-Shakin-Thaler (EST) method. In all cases the potentials generate phase shifts that fit well the low energy experimental data.

PACS Numbers: 21.45+v, 21.30.-x, 21.60.Gx, 25.10+s

I. INTRODUCTION

^{3}He plays an important role in a variety of light-cluster reactions, especially at low energies. One such reaction is ^{3}He(d,p)^{4}He which is of interest in primordial nucleosynthesis studies and in studies related to the abundance of elements in the Universe. It is also of interest as a fusion reaction, as it generates no neutrons. At medium energies, this reaction with polarized spins has been used to constrain the deuteron D-state probability [1]. Another interesting aspect of this reaction is that the ^{3}He nucleus behaves like a neutron, because the proton pair in ^{3}He almost forms a closed shell structure and therefore ^{3}He can serve as a good substitute for a neutron target.

The ^{3}He(d,p)^{4}He reaction can be modeled as a three-body p–n–^{3}He problem which can be handled using the Faddeev formalism [2–4]. This presupposes a knowledge of the p–^{3}He and the n–^{3}He interactions and of the nuclear potential. The nucleon-trinucleon interaction

*Email address: oryu@ph.noda.sut.ac.jp

has been the subject of several investigations in the past. Despite the effort made, the interaction is far from being understood. Many questions concerning the range and shape of the potential, as well as its energy–, parity-, and ℓ-dependence. For example, in the optical model approach the shape is either pre-chosen (Woods-Saxon [5], Gaussian [6] *etc.*) or is fitted to specific scattering cross sections [7,8], or to phase shifts which are used as input to construct phase equivalent local potentials via inverse scattering methods [9]. Some experimental data on p–^{3}He elastic scattering up to $\sim$ 10 MeV were analyzed within the framework of a separable potential model, phase shifts for the p–^{3}He and n–^{3}H systems were generated [10].

The quality of scattering data used as input and their reproducibility is another source of ambiguity for the field practitioner. Extensive phase shift analyses for the nucleon-trinucleon system were performed in the 1960s and 1970s [11–18]. The most recent was carried out by Yoshino *et al.* [19] in the E_p = 4.0-19.48 MeV energy region. As was pointed out, in Ref. [9], performing phase shift analyses and constructing a potential in a specific channel requires extreme care to insure that the interaction has the correct energy–, parity-, and ℓ-dependence. The mere use of cross sections is not sufficient to uniquely extract all of these dependencies. An alternative scheme is to generate the phase shifts from reliable theoretical models, such as the Resonating Group Model (RGM). Within the RGM formalism, Reichstein *et al.* [20] extracted the intercluster phase shifts for this system while Furutani *et al.* [21] calculated the phase shifts by using the Generator Coordinate Method (GCM). Their results are in good agreement with the differential cross section and the polarization data in the low energy region. Although the calculated energy spectrum of the $T = 1$ resonances fits equally well the experimental data [12], these experimental data have been replaced in the recent article by Tilley *et al.* [22]. Finally, we mention that an optical potential approach has been employed by Teshigawara *et al.* [23] to study the n–^{3}He system within the Complex Scaled Siegert Method.

In this paper, we employ the p–^{3}He nonlocal RGM interaction [20,24] and its variant version, the so-called Orthogonality Condition Model (OCM) in which the Pauli forbidden states (PFS) are removed [25,26]. Furthermore, to reproduce the experimental phase shifts sufficiently well and to treat the degenerate states stemming from the absence of LS forces from the RGM kernel, we have introduced phenomenological LS forces using a technique similar to that of Ref. [27]. Tensor forces could also be considered for the $^3S_1$-$^3D_1$, $^1P_1$-$^3P_1$, $^3P_2$-$^3F_2$, and $^1D_2$-$^3D_2$ channels. However, the corresponding experimental mixing parameters were found to be negligibly small [19] and therefore they have been omitted.

At higher energies, the absorptive part of the phase shifts could be important, in which case an imaginary part should be included in the potential. However, in a recent phase shift analysis of Yoshino *et al.* [19], neither the reflection parameters for the coupling effects in different particle channels nor the imaginary part of the phase shifts above the break-up threshold were found to be significant. Therefore, we will not consider the construction of complex p–^{3}He potentials and concentrate instead on real potentials that fit the low energy experimental data well.

Finally, we have endeavored to represent the potentials, that reproduce the phase shifts without Coulomb effects, in a separable form with appropriate form factors and parameters by using the Ernst-Shakin-Thaler (EST) method [28]. Such potentials are useful in solving the three-body Faddeev equations in momentum space.

In Sec. II we describe our methods to construct the p-^{3}He potential and in Sec. III we present our results. In Sec. IV we present the separable expansions for the p-^{3}He potentials while in Sec. V we present our discussions and conclusions. Finally, some technical details and formulas are shifted in Appendices A and B.

II. THE p - ^{3}He POTENTIAL

The construction of our p–^{3}He effective potential is based on the RGM formalism, which is given in configuration space in the paper by Reichstein *et al.* [20]. In operator form the RGM potential is

$$V^{\rm RGM} \equiv W + E\mathcal{N}, \tag{2.1}$$

where W is the energy independent local and nonlocal potential, E is the relative energy between the proton and ^{3}He while $\mathcal{N}$ is the norm (-integral) kernel (see Appendix A for details).

A common problem encountered in the RGM formalism is the existence of the PFS which can be removed via the OCM technique (see Appendix A). The OCM potential is given by

$$V^{\rm OCM} = \frac{1}{\sqrt{1-\mathcal{N}}}\,(\,h_0 + W\,)\,\frac{1}{\sqrt{1-\mathcal{N}}} - h_0 \tag{2.2}$$

where h_0 is the kinetic energy operator between the proton and ^{3}He. It should be noted that $V^{\rm OCM}$ is an energy independent potential.

The above operator equations can be brought into a more concrete form by using the eigen-values γ_i and the eigen-functions $\tilde{U}_i$ of the norm kernel,

$$V^{\rm OCM} = \sum_{ij=1}^{\infty} |\tilde{U}_i\rangle[\frac{1}{\sqrt{1-\gamma_i}}(h_{0ij}+W_{ij})\frac{1}{\sqrt{1-\gamma_j}} - h_{0ij}]\langle\tilde{U}_j| \tag{2.3}$$

with

$$\mathcal{N}|\tilde{U}_i\rangle = \gamma_i|\tilde{U}_i\rangle \tag{2.4}$$

and with matrix elements $W_{ij} = \langle\tilde{U}_i|\,W\,|\tilde{U}_j\rangle$ and $h_{0ij} = \langle\tilde{U}_i|\,h_0\,|\tilde{U}_j\rangle$. We solved Eq.(2.4) to obtain the eigen-value γ_i and the eigen-function $\tilde{U}_i$ for each state of the p–^{3}He system up to a large number $i = N_s$, beyond which the eigen-functions $\tilde{U}_i$ become highly oscillatory. These oscillations make the numerical calculations cumbersome and unstable.

The eigen-functions $\tilde{U}_i$ can be expressed in terms of harmonic oscillator functions U_i (see Eq. (A18)). Since the potential V^{OCM} becomes infinite for a PFS($\gamma_i = 1$) the corresponding wave function is removed from the eigen-functions of the Schrödinger equation. For the partly PFS ($0 < \gamma_i < 1$) we note that the eigen-values γ_i converge quickly to zero as i increases and thus for a sufficiently large number N_S,

$$V^{\rm OCM} \rightarrow \sum_{ij=N_S}^{\infty} |\tilde{U}_i\rangle W_{ij}\langle\tilde{U}_j|. \tag{2.5}$$

Therefore, by using $W = \sum_{ij=1}^{\infty} |\tilde{U}_i\rangle W_{ij} \langle \tilde{U}_j| = V^{RGM}(E=0)$, we obtain instead of Eq. (2.3) the modified OCM (MOCM) potential

$$
\begin{aligned}
V^{\rm MOCM} &= W - \sum_{ij=1}^{\infty} |\tilde{U}_i\rangle W_{ij} \langle \tilde{U}_j| + \sum_{ij=N_S}^{\infty} |\tilde{U}_i\rangle W_{ij} \langle \tilde{U}_j| \\
&+ \sum_{ij=1}^{N_S} |\tilde{U}_i\rangle [\frac{1}{\sqrt{1-\gamma_i}} (h_{0ij} + W_{ij}) \frac{1}{\sqrt{1-\gamma_j}} - h_{0ij}] \langle \tilde{U}_j| \\
&= V^{RGM}(E=0) + \sum_{ij=1}^{N_S} |\tilde{U}_i\rangle \Big[\frac{1}{\sqrt{1-\gamma_i}} (h_{0ij} + W_{ij}) \frac{1}{\sqrt{1-\gamma_j}} - (h_{0ij} + W_{ij}) \Big] \langle \tilde{U}_j|. \quad (2.6)
\end{aligned}
$$

If the number of PFS is N_F then from the orthogonality condition between $\langle \tilde{U}_j|$ and the physical wave function $|\psi\rangle$, given by Eq. (A11), we obtain

$$
\Big(\sum_{ij=1}^{N_F} |\tilde{U}_i\rangle \Big[\frac{1}{\sqrt{1-\gamma_i}} (h_{0ij} + W_{ij}) \frac{1}{\sqrt{1-\gamma_j}} - (h_{0ij} + W_{ij}) \Big] \langle \tilde{U}_j| \Big) |\psi\rangle = 0. \quad (2.7)
$$

Thus, the part of the potential in Eq.(2.6) has no effect in the Schrödinger equation. Consequently, we introduce our MOCM potential as follows,

$$
V^{\rm MOCM} \equiv V^{RGM}(E=0) + \sum_{ij=N_F+1}^{N_S} |\tilde{U}_i\rangle \Big[\frac{1}{\sqrt{1-\gamma_i}} (h_{0ij} + W_{ij}) \frac{1}{\sqrt{1-\gamma_j}} - (h_{0ij} + W_{ij}) \Big] \langle \tilde{U}_j|. \quad (2.8)
$$

For the $\ell = 0$ state of the p-^{3}He system, the eigenvalues γ_i are γ_1= 0.98993, γ_2= 0.12020, γ_3= 0.01373, and so on, *i.e.* there are no PFS in the system. For higher partial waves, the absolute values of γ_i are much less than one, and therefore $N_F = 0$ as well. Thus, Eq. (2.8) is not only free from a diverging term caused by $\gamma_i = 1$, but also from numerical errors due to presence of oscillator functions with higher frequencies.

Each term of Eq.(2.8) can be easily transformed into its momentum space using Fourier transforms (see Appendix B). It is found that the on-shell parts of the OCM scattering amplitude obtained with the transformed potentials are almost the same as those of the RGM amplitude, although the off-shell parts differ. For the spin-triplet P- and D- waves and with $N_S = 20$ the resulting phase shift differ slightly. However, the differences are small enough and do not give rise to any important effects in the parameter fitting of these triplet channels.

Within the above formalism, a realistic force with an LS component has rarely been considered until now [29]. As a consequence, the intercluster p–^{3}He potential of the MOCM, Eq. (2.8), does not include an LS force either. Although in the RGM formalism the NN interaction could include an LS and tensor force, this may necessitate some additional antisymmetrization procedure. However, if we adopt a proper intrinsic cluster function that includes the effects of these forces, we could include these effects in the inter-cluster potentials by means of a folding procedure. In previous work McIntyre and Haeberli [27] introduced a phenomenological LS force to reduce the degeneracy of the L-induced potentials. In the present work we use the same technique but with an extended form for the LS forces. The LS dependence in the intercluster potentials for the spin-triplet channels is introduced via

$$V^{\rm OCM(LS)} = \{C_0 + C_1 \boldsymbol{L}\cdot\boldsymbol{S} + C_2(\boldsymbol{L}\cdot\boldsymbol{S})^2 + C_3(\boldsymbol{L}\cdot\boldsymbol{S})^3\} V^{\rm MOCM}, \tag{2.9}$$

where C_0, C_1, C_2,and C_3 are parameters adjusted to fit the experimental phase shifts. For now on we shall, for simplicity, use from now on the abbreviation OCM instead of MOCM. The parameters for the p–^{3}He interactions are shown in Table.I.

TABLES

TABLE I. Parameters of the p–^{3}He interactions.

State	C_0	C_1	C_2	C_3
$^3P_0$ $^3P_1$ $^3P_2$	1.2080	0.0788	−0.0740	−0.0110
$^3D_1$ $^3D_2$ $^3D_3$	0.9780	0.0446	0.0616	−0.0090
$^3F_2$ $^3F_3$ $^3F_4$	1.2000	0.0360	0.0084	0.0000

Tensor forces should be considered, in principle, for the $^3S_1$-$^3D_1$, $^1P_1$-$^3P_1$, $^3P_2$-$^3F_2$, and $^1D_2$-$^3D_2$ coupled channels. However, as mentioned in the introduction, in the phase-shift analysis by Yoshino *et. al.* [19] it was found that the mixing parameters for the p–^{3}He interaction are very small; *i.e.*, $\varepsilon_1^+ = -0.2719 \pm 0.0097\,\mathrm{deg}$, $\varepsilon_1^- = -0.4001 \pm 0.3490\,\mathrm{deg}$, $\varepsilon_2^+ = -0.0269 \pm 0.2510\,\mathrm{deg}$, and $\varepsilon_2^- = 0.0827 \pm 0.0129\,\mathrm{deg}$ at $E_p = 19.48\,\mathrm{MeV}$ for the $^3S_1$-$^3D_1$, $^1P_1$-$^3P_1$, $^1D_2$-$^3D_2$, and $^3P_2$-$^3F_2$ partial waves, respectively. Therefore, tensor forces were omitted.

III. PHASE SHIFT CALCULATIONS

The p-^{3}He phase shifts were calculated using the program "GSE" developed in Refs. [30,31]. The GSE method is one generalization of Bateman's method in which the on-shell and half-off-shell properties of the t-matrix are exact when the on-shell momentum is chosen to be the Bateman parameter. In order to take into account the Coulomb interaction for the p-^{3}He system, Reichstein *et al.* introduced a kind of Coulomb force in the RGM formalism which takes the form of an Error function [20]. In momentum representation, the Error function can be expanded in the short range region in terms of Gaussian functions while in the long range region it can be expressed in terms of a Coulomb potential between the ^{3}He cluster and the proton. In order to obtain the phase-shift modification by the Coulomb interaction, we adopt a screened Coulomb potential of the Yukawa type. The difference between the pure Coulomb and the screened Coulomb potential in the long range region is corrected by means of a renormalization technique [32].

The screened Coulomb potential is defined by

$$V^R(r) = \frac{ZZ'e^2}{r}\exp(-r/R) \tag{3.1}$$

where R is called the screened Coulomb range parameter which, in our case, has the value of $R = 810.753\,\mathrm{fm}$ for S-wave, $R = 1128.677\,\mathrm{fm}$ for P-wave, $R = 1439.062\,\mathrm{fm}$ for D-wave, and $R = 10158.163\,\mathrm{fm}$ for F-wave. The partial wave expansion of V^R, in momentum space, is given by

$$V_\ell^R(k,k') = 2\pi\frac{ZZ'e^2}{kk'}Q_\ell\Big(\frac{k^2+k'^2+1/R^2}{2kk'}\Big) \tag{3.2}$$

where $Q_\ell(x)$ is the Legendre function of the second kind. The calculated screened Coulomb phase shift $\delta_\ell^R(k)$ using Eq. (3.2) is given by

$$\delta_\ell^R(k) = \sigma_\ell(k) - \phi(k,R) \tag{3.3}$$

where $\sigma_\ell(k)$ is the Coulomb phase, $\phi(k,R)$ is the renormalization phase given by $\phi(k,R) = \eta(\ln 2kR - \gamma) + \cdots$, η is the Sommerfeld parameter $\eta = \mu ZZ'e^2/k$, μ is a reduced mass, and γ is the Euler constant $\gamma = 0.5772156\cdots$.

In order to calculate the Coulomb modified nuclear phase shifts δ_ℓ^{SC}, we first put the total potential with the short range nuclear part $V^{\mathrm{OCM(LS)}}$ and the Coulomb part into partial wave form,

$$V_\ell(k,k') = V_\ell^{\mathrm{OCM(LS)}}(k,k') + V_\ell^R(k,k'). \tag{3.4}$$

Then, the calculated total phase shift is given by

$$\delta_\ell^{(R)} \equiv \delta_\ell^{SR} + \delta_\ell^R(k) = \delta_\ell^{SR}(k) + \sigma_\ell(k) - \phi(k,R). \tag{3.5}$$

Consequently the Coulomb modified nuclear phase shift $\delta_\ell^{SR}(k)$ is

$$\begin{aligned} \delta_\ell^{SR}(k) &= \delta_\ell^{(R)} - \delta_\ell^R(k) \\ &= \delta_\ell^{(R)}(k) + \phi(k,R) - \sigma_\ell(k). \end{aligned} \tag{3.6}$$

The genuine Coulomb modified nuclear phase shifts are obtained via Eq. (3.6) in the long range limit,

$$\begin{aligned} \delta_\ell^{SC}(k) &= \lim_{R\to\infty} [\delta_\ell^{(R)} + \phi(k,R)] - \sigma_\ell(k) \\ &= \delta_\ell(k) - \sigma_\ell(k), \end{aligned} \tag{3.7}$$

where $\delta_\ell(k)$ is the total phase shift generated by the nuclear plus Coulomb potentials. The results, for the ^{1}S$_0$, ^{3}S$_1$ partial waves, are shown in Fig. 1 and compared with the results of the phase shift analyses [10,19,11,12,14–17]. It is seen that the phase shifts for these channels are well reproduced. This confirms the on-shell equivalence of the OCM and the RGM potentials.

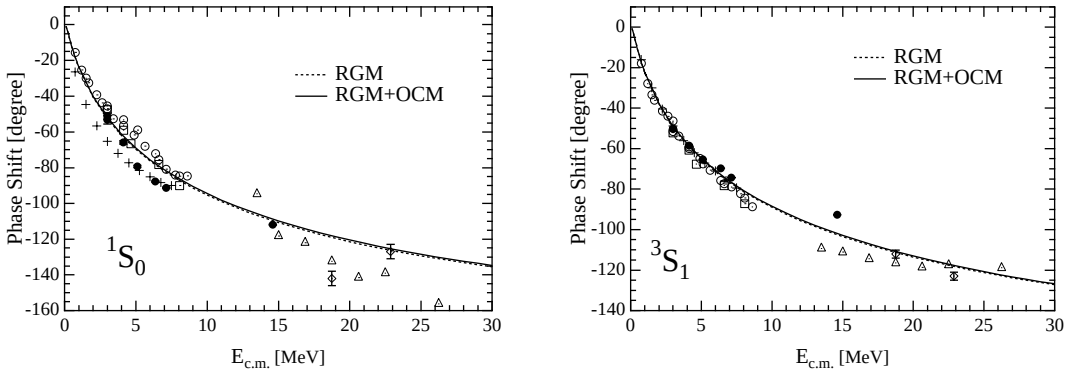

FIG. 1. p-^{3}He phase shifts for the $^1S_0$ and $^3S_1$ partial waves. The experimental data are: ○ Tombrello [12] □ Mc Sherry and Baker [14], △ Morales *et al.* [16], ◇ Müller *et al.* [17], + Beltramin *et al.* [10], and • Yoshino *et al.* [19]. The dashed line denotes the RGM and the solid line the RGM+OCM results, respectively.

In Fig. 2, the phase shifts for the $^1P_0$, $^3P_0$, $^3P_1$, $^3P_2$ partial waves are shown. The spin singlet $^1P_0$ phases for the RGM and the RGM+OCM potentials are obtained without an LS force. In contrast, the $^3P_0$, $^3P_1$, $^3P_2$ partial waves are spin triplet, and therefore the LS force is taken into account. It is seen that our results are in very good agreement with the experimental data, especially for energies below 10 MeV. This demonstrates the importance of the LS force in the potential.

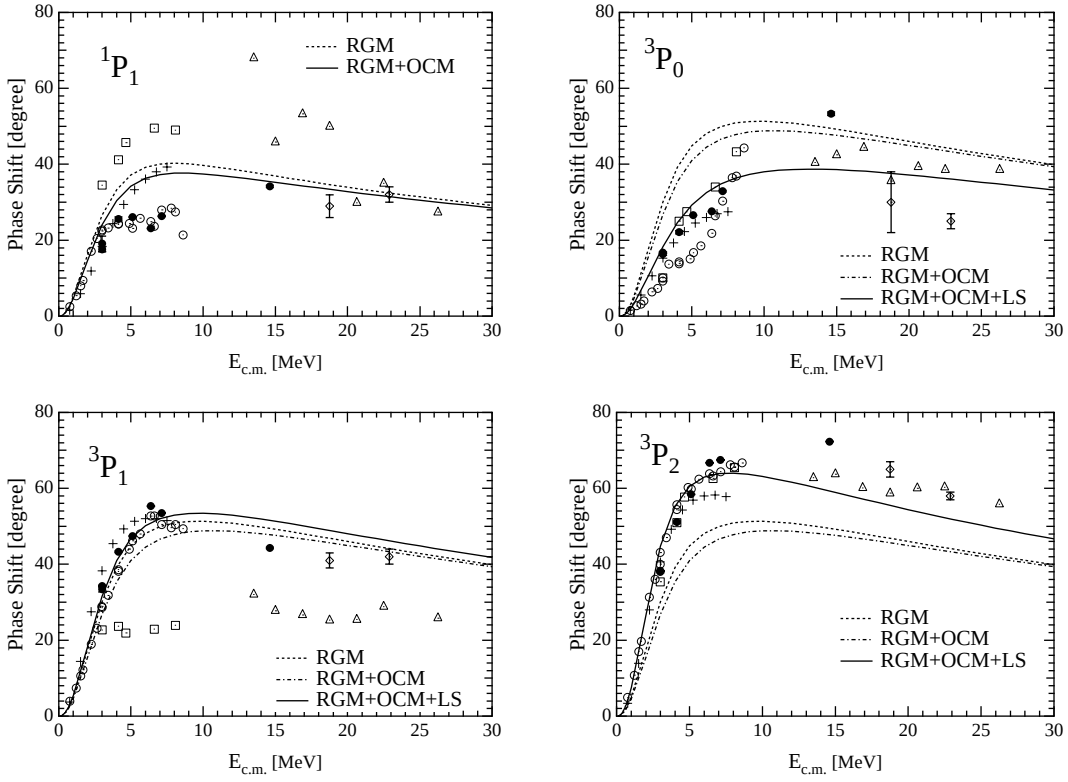

FIG. 2. p-^{3}He phase shifts for the $^1P_1$, $^3P_0$, $^3P_1$, and $^3P_2$ partial waves. Symbols for the experimental data are the same as in Fig. 1. For the singlet channel the dashed line denotes the RGM and the solid line the RGM+OCM results. For the triplet channel the dashed line denotes the RGM, the dashed-dotted line the RGM+OCM, and the solid lines the RGM+OCM+LS results, respectively.

In Fig. 3 the phase shifts for $^1D_2$, $^3D_1$, $^3D_2$, and $^3D_3$ partial waves are shown. The spin-singlet $^1D_2$ partial wave is calculated using the RGM+OCM potential without inclusion of an LS force. Once again, the results are in good agreement with the experimental data of Yoshino *et al.* [19] in the lower energy region. It should be noted that, unlike for the P wave results, the LS force is less important for the $^3D_1$, $^3D_2$, and $^3D_3$ partial waves.

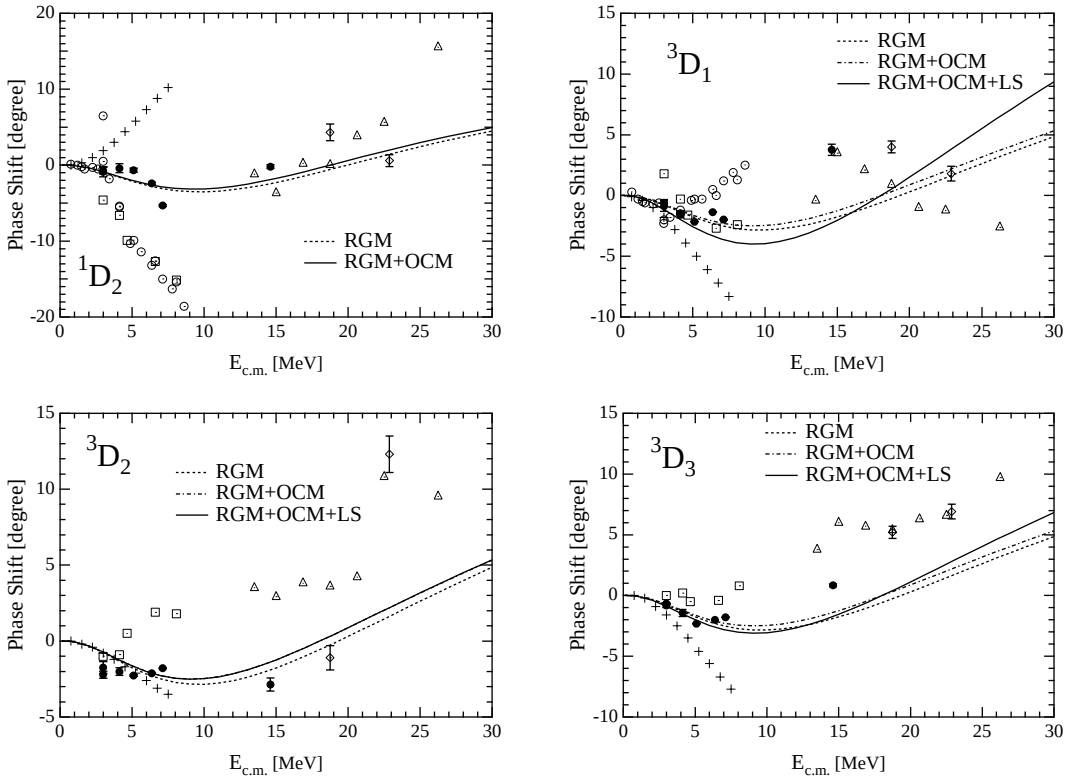

FIG. 3. p-^{3}He phase shifts for the $^1D_2$, $^3D_1$, $^3D_2$, and $^3D_3$ partial waves. The notation is the same as in Fig. 1 and 2.

In Fig. 4, the $^1F_3$, $^3F_2$, $^3F_3$, and $^3F_4$ partial wave phase shifts are shown. Again, the $^1F_3$ is a spin singlet. The results were obtained using the RGM and RGM+OCM potentials only. In order to obtain the relevant constants for the LS force in the $^3F_2$, $^3F_3$, and $^3F_4$ channels, we employed the latest experimental data by Yoshino *et al.* [19].

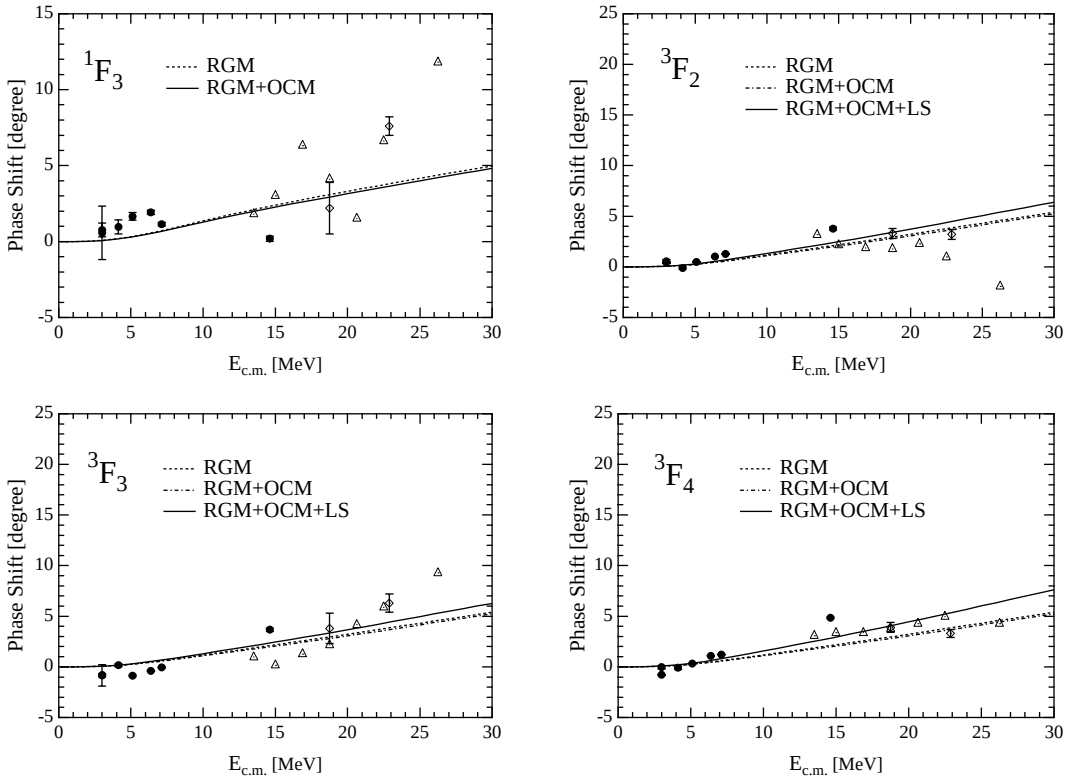

FIG. 4. p-^{3}He phase shifts for the ^{1}F$_3$, ^{3}F$_2$, ^{3}F$_3$, ^{3}F$_4$ partial waves. The notation is the same as in Fig. 1 and 2.

IV. SEPARABLE EXPANSION OF THE p-^{3}He POTENTIALS

In order to be useful the potential $V^{OCM(LS)}$ must be converted into a separable expansion form. To achieve this we employed the EST separable expansion method [28] which is briefly described below.

The EST rank N separable potential $V^{\rm EST}(p,p')$ is defined in terms of the form factor $g_i(p)$ and the coupling constant λ_{ij}

$$V^{\rm EST}(p,p') = \sum_{i,j=1}^{N} g_i(p)\,\lambda_{ij}\,g_j(p')\,. \tag{4.1}$$

The form factor is given by the R-matrix,

$$g_i(p) = \langle p|V|\Psi(E_i)\rangle \equiv R(p,k_i;E_i), \tag{4.2}$$

where E_i is a fixed energy point and k_i is the on-shell momentum at this energy. The expansion energies used are E_1=1MeV for the rank-1 case, and E_1=1MeV, E_2=10MeV, and E_3=15MeV for the rank-3 case.

The R-matrix satisfies the equation

$$\begin{aligned} R(p,k_i;E_i) &= V(p,k_i) + \mathcal{P}\int_0^\infty V(p,p')G_0(p';E_i)R(p',k_i;E_i)\frac{p'^2}{2\pi^2}\,{\rm d}p' \\ &= V(p,k_i) + \mathcal{P}\int_0^\infty \frac{V(p,p')R(p',k_i;E_i)}{E_i - p'^2/2\mu}\frac{p'^2}{2\pi^2}\,{\rm d}p' \end{aligned} \tag{4.3}$$

where $\mathcal{P}$ denotes the principal value integral. For practical reasons the form factor $g_i(p)$ is expanded in terms of polynomials,

$$g_n(p) = e^{-\beta p^2} p^l \sum_{m=1}^{20} a_{n,m} p^{2(m-1)} \,, \tag{4.4}$$

where $\beta = 1/0.825$ and $a_{n,m}$ are fitting parameters.

The coupling constant λ_{ij} is defined by

$$(\lambda^{-1})_{ij} = \langle \Psi(E_i)|V|\Psi(E_j)\rangle = R(k_i,k_j;E_i) + \mathcal{P}\int_0^\infty R(k_i,p;E_i) G_0(p;E_i) R(p,k_j;E_i) \frac{p^2}{2\pi^2}\,\mathrm{d}p. \tag{4.5}$$

A. Singlet channel

The singlet p–^{3}He potential does not contain an LS force. We endeavored to construct two different p–^{3}He potentials, one of rank-1 and the other of rank-3. The rank-1 parameters for the form factor are the same as those of the first term of the rank-3 but the coupling constant is different.

The parameters for these potentials for the ^{1}S$_0$ state are given in Tables II and III while the phase shift results are presented in Fig. 5. It is seen that the difference between the phase shifts, especially in the lower energy region, is very small.

TABLE II. Parameters $a_{n,m}$ of the form factor of Eq. (4.4) for the ^{1}S$_0$ potential. The first column lists the rank-1 parameters with $\lambda_{11} = 2.976586$.

$a_{1,m}$	$a_{2,m}$	$a_{3,m}$
0.81290761×10^{1}	-0.37821814×10^{2}	-0.13596682×10^{2}
-0.13818233×10^{2}	0.45121340×10^{2}	0.14012550×10^{2}
0.26993988×10^{2}	-0.86975431×10^{2}	-0.27226075×10^{2}
-0.29584805×10^{2}	0.78262662×10^{2}	0.21711608×10^{2}
0.22158774×10^{2}	-0.47493102×10^{2}	-0.11624436×10^{2}
-0.12179712×10^{2}	0.20523082×10^{2}	0.42622121×10^{1}
0.52046713×10^{1}	-0.68468420×10^{1}	-0.11659454×10^{1}
-0.17809791×10^{1}	0.18744208×10^{1}	0.26053262
0.49289681	-0.44089876	-0.54300629×10^{-1}
-0.11013105	0.90888217×10^{-1}	0.11621725×10^{-1}
0.19710935×10^{-1}	-0.16177816×10^{-1}	-0.23952017×10^{-2}
-0.27963987×10^{-2}	0.23984064×10^{-2}	0.41701960×10^{-3}
0.31072739×10^{-3}	-0.28510226×10^{-3}	-0.56522712×10^{-4}
-0.26665392×10^{-4}	0.26325182×10^{-4}	0.57510182×10^{-5}
0.17360057×10^{-5}	-0.18369762×10^{-5}	-0.43035052×10^{-6}
-0.83650320×10^{-7}	0.94090317×10^{-7}	0.23179820×10^{-7}
0.28751338×10^{-8}	-0.34035371×10^{-8}	-0.86968112×10^{-9}
$-0.66353945\times10^{-10}$	0.81822792×10^{-10}	0.21475347×10^{-10}

0.91778681×10^{-12}	$-0.11672988\times10^{-11}$	$-0.31250844\times10^{-12}$
$-0.57298542\times10^{-14}$	0.74478363×10^{-14}	0.20237810×10^{-14}

TABLE III. Coupling constants $\lambda_{ij} = \lambda_{ji}$ of the rank–3 $^1S_0$ potential.

$\lambda_{11} = -0.12888040\times10^{2}$
$\lambda_{12} = -0.12924909\times10^{2}$
$\lambda_{13} = 0.25638703\times10^{2}$
$\lambda_{22} = -0.11179525\times10^{2}$
$\lambda_{23} = 0.21826395\times10^{2}$
$\lambda_{33} = -0.42790529\times10^{2}$

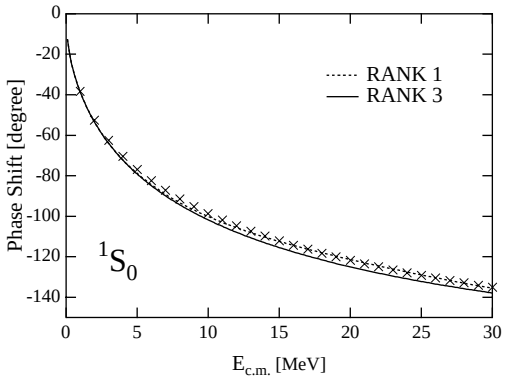

FIG. 5. Phase shifts for the $^1S_0$ partial wave without the Coulomb effects. The crosses denote the RGM+OCM results, the dashed line the rank-1 result, and the solid line the rank-3 result, respectively.

The results for the $^1P_1$ channel are given in Tables IV and V while the phase shifts are given in Fig. 6. As can be seen from this figure the rank-1 potential fails to reproduce the results beyond ~ 4 MeV. Similar results were obtained for the $^1D_2$ and $^1F_3$ channels. These results are presented in Tables VI-IX and plotted in Figs. 7-8.

TABLE IV. Parameters $a_{n,m}$ of the form factor of Eq. (4.4) for the $^1P_1$ potential. The first column exhibits the rank-1 parameters with $\lambda_{11} = -0.29317504$.

$a_{1,m}$	$a_{2,m}$	$a_{3,m}$
-0.94249747$\times 10^{1}$	-0.80751728$\times 10^{1}$	-0.54943593$\times 10^{1}$
0.16850309$\times 10^{2}$	0.72033423$\times 10^{1}$	0.28748548$\times 10^{1}$
-0.25259235$\times 10^{2}$	-0.90782035$\times 10^{1}$	-0.33647532$\times 10^{1}$
0.22361127$\times 10^{2}$	0.46110606$\times 10^{1}$	0.41169528
-0.14005952$\times 10^{2}$	-0.13188315$\times 10^{1}$	0.60064787
0.67212849$\times 10^{1}$	0.16478322	-0.41395211
-0.26035140$\times 10^{1}$	-0.27097734$\times 10^{-1}$	0.86574730$\times 10^{-1}$
0.83231138	0.41703584$\times 10^{-1}$	0.28862915$\times 10^{-1}$
-0.22037742	-0.29197374$\times 10^{-1}$	-0.28632910$\times 10^{-1}$
0.47917437$\times 10^{-1}$	0.11484498$\times 10^{-1}$	0.11370739$\times 10^{-1}$
-0.84391784$\times 10^{-2}$	-0.29953237$\times 10^{-2}$	-0.29062500$\times 10^{-2}$
0.11860729$\times 10^{-2}$	0.55358368$\times 10^{-3}$	0.52610797$\times 10^{-3}$
-0.13104955$\times 10^{-3}$	-0.74563678$\times 10^{-4}$	-0.69658876$\times 10^{-4}$
0.11203792$\times 10^{-4}$	0.73865049$\times 10^{-5}$	0.68075554$\times 10^{-5}$
-0.72718918$\times 10^{-6}$	-0.53624860$\times 10^{-6}$	-0.48896135$\times 10^{-6}$
0.34933248$\times 10^{-7}$	0.28090702$\times 10^{-7}$	0.25397873$\times 10^{-7}$
-0.11963972$\times 10^{-8}$	-0.10294665$\times 10^{-8}$	-0.92452666$\times 10^{-9}$
0.27487008$\times 10^{-10}$	0.24947694$\times 10^{-10}$	0.22283655$\times 10^{-10}$
-0.37800739$\times 10^{-12}$	-0.35784010$\times 10^{-12}$	-0.31823024$\times 10^{-12}$
0.23427534$\times 10^{-14}$	0.22924616$\times 10^{-14}$	0.20314053$\times 10^{-14}$

TABLE V. Coupling constants $\lambda_{ij} = \lambda_{ji}$ of the rank-3 $^1\mathrm{P}_1$ potential.

λ_{11} =-0.86234010$\times 10^1$
λ_{12} = 0.26099258$\times 10^2$
λ_{13} =-0.24411307$\times 10^2$
λ_{22} =-0.88300863$\times 10^2$
λ_{23} = 0.85424554$\times 10^2$
λ_{33} =-0.83781354$\times 10^2$

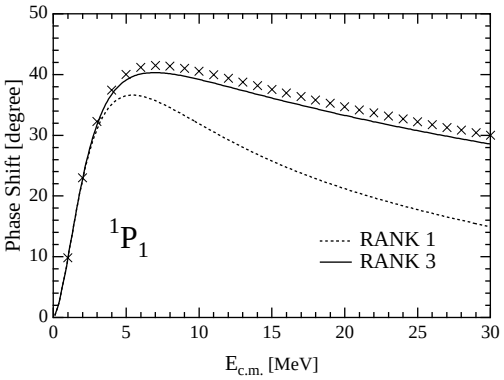

FIG. 6. Phase shifts for the $^1P_1$ partial wave without Coulomb effects. The crosses denote the RGM+OCM result, the dashed line the rank-1 result, and the solid line the rank-3 result, respectively.

TABLE VI. Parameters $a_{n,m}$ of the form factor of Eq. (4.4) for the $^1D_2$ potential. The first column gives the rank-1 parameters with $\lambda_{11} = 0.49171217\times10^2$

$a_{1,m}$	$a_{2,m}$	$a_{3,m}$
0.68105470	0.19763270×10^1	0.16194259×10^1
-0.19186565×10^1	-0.54138849×10^1	-0.45399709×10^1
0.27889420×10^1	0.67678908×10^1	0.50617192×10^1
-0.25046661×10^1	-0.50530126×10^1	-0.33071540×10^1
0.15881034×10^1	0.26186515×10^1	0.14542318×10^1
-0.76207628	-0.10174428×10^1	-0.45838231
0.28729893	0.31100450	0.10636485
-0.86461811×10^{-1}	-0.76634068×10^{-1}	-0.17716414×10^{-1}
0.20858825×10^{-1}	0.15393708×10^{-1}	0.18712562×10^{-2}
-0.40260171×10^{-2}	-0.25251882×10^{-2}	-0.43762336×10^{-4}
0.61860736×10^{-3}	0.33681168×10^{-3}	-0.26015437×10^{-4}
-0.75152221×10^{-4}	-0.36220702×10^{-4}	0.57462271×10^{-5}
0.71556851×10^{-5}	0.31045680×10^{-5}	-0.69663479×10^{-6}
-0.52783394×10^{-6}	-0.20899733×10^{-6}	0.57050021×10^{-7}
0.29679582×10^{-7}	0.10841787×10^{-7}	-0.32922530×10^{-8}
-0.12425007×10^{-8}	-0.42224769×10^{-9}	0.13358706×10^{-9}
0.37349976×10^{-10}	0.11883187×10^{-10}	$-0.37020130\times10^{-11}$
$-0.75924107\times10^{-12}$	$-0.22720832\times10^{-12}$	0.65926451×10^{-13}
0.93178858×10^{-14}	0.26314644×10^{-14}	$-0.66816378\times10^{-15}$
$-0.51997857\times10^{-16}$	$-0.13885275\times10^{-16}$	0.28516854×10^{-17}

TABLE VII. Coupling constants $\lambda_{ij} = \lambda_{ji}$ for the rank-3 $^1D_2$ potential.

$\lambda_{11} = 0.23985939\times10^4$
$\lambda_{12} =$-0.13537297$\times10^4$
$\lambda_{13} = 0.66626420\times10^3$
$\lambda_{22} = 0.74471421\times10^3$
$\lambda_{23} =$-0.34111641$\times10^3$
$\lambda_{33} = 0.13709213\times10^3$

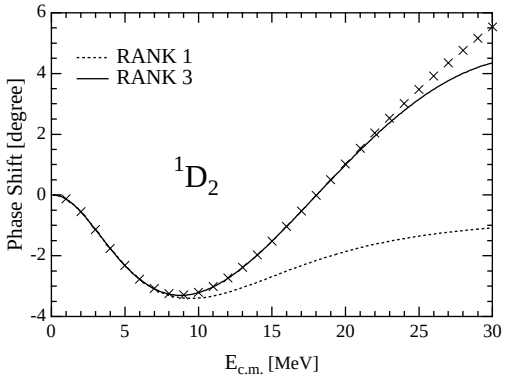

FIG. 7. Phase shifts for the $^1D_2$ partial waves without Coulomb effects. The crosses denote the RGM+OCM result, the dashed line the rank-1 result, and the solid line the rank-3 result, respectively.

TABLE VIII. Parameters $a_{n,m}$ of the form factor of Eq. (4.4) for the $^1F_3$ potential. The first column lists the rank-1 parameters with λ_{11} =-0.157512965$\times 10^4$.

$a_{1,m}$	$a_{2,m}$	$a_{3,m}$
-0.10309579	-0.10491693$\times 10^1$	-0.10971956$\times 10^1$
0.25614578	0.21551217$\times 10^1$	0.19720076$\times 10^1$
-0.35470074	-0.26919503$\times 10^1$	-0.23113579$\times 10^1$
0.30827988	0.20398472$\times 10^1$	0.15842458$\times 10^1$
-0.18968846	-0.10780556$\times 10^1$	-0.73781489
0.88041294$\times 10^{-1}$	0.42456486	0.24470228
-0.31866032$\times 10^{-1}$	-0.12903376	-0.57371456$\times 10^{-1}$
0.91323183$\times 10^{-2}$	0.30698165$\times 10^{-1}$	0.84797207$\times 10^{-2}$
-0.20840227$\times 10^{-2}$	-0.57388079$\times 10^{-2}$	-0.30810984$\times 10^{-3}$
0.37892090$\times 10^{-3}$	0.84146200$\times 10^{-3}$	-0.20824797$\times 10^{-3}$
-0.54767188$\times 10^{-4}$	-0.96337919$\times 10^{-4}$	0.63773382$\times 10^{-4}$
0.62640005$\times 10^{-5}$	0.85660575$\times 10^{-5}$	-0.10605018$\times 10^{-4}$
-0.56298706$\times 10^{-6}$	-0.58902484$\times 10^{-6}$	0.11988500$\times 10^{-5}$
0.39349866$\times 10^{-7}$	0.31325432$\times 10^{-7}$	-0.97107918$\times 10^{-7}$
-0.21061797$\times 10^{-8}$	-0.13004858$\times 10^{-8}$	0.56943638$\times 10^{-8}$
0.84350422$\times 10^{-10}$	0.42992976$\times 10^{-10}$	-0.23915836$\times 10^{-9}$
-0.24379678$\times 10^{-11}$	-0.11462659$\times 10^{-11}$	0.69843623$\times 10^{-11}$
0.47882660$\times 10^{-13}$	0.23655180$\times 10^{-13}$	-0.13400069$\times 10^{-12}$
-0.57032237$\times 10^{-15}$	-0.32743658$\times 10^{-15}$	0.15094646$\times 10^{-14}$
0.31009923$\times 10^{-17}$	0.21752827$\times 10^{-17}$	-0.75136464$\times 10^{-17}$

TABLE IX. Coupling constants $\lambda_{ij} = \lambda_{ji}$ for the rank-3 $^1\mathrm{F}_3$ potential.

λ_{11} =-0.11253575$\times 10^6$
λ_{12} = 0.26062364$\times 10^5$
λ_{13} =-0.14514498$\times 10^5$
λ_{22} =-0.63200447$\times 10^4$
λ_{23} = 0.35959447$\times 10^4$
λ_{33} =-0.20743460$\times 10^4$

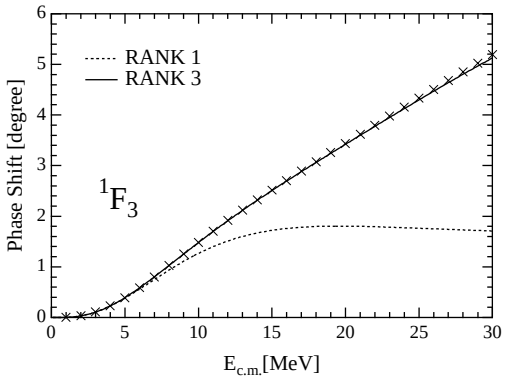

FIG. 8. Phase shifts for $^1F_3$ partial wave without Coulomb effects. The crosses denote the RGM+OCM result, the dashed line the rank-1 result, and the solid line the rank-3 result, respectively.

B. Triplet Channel

The parameters for the spin–triplet partial waves $^3S_1$ ($^3P_0$,$^3P_1$, $^3P_2$), ($^3D_1$, $^3D_2$,$^3D_3$), and ($^3F_2$, $^3F_3$,$^3F_4$), are given in Tables X-XXIX while the phase shifts are given in Figs. 9-18. In the case of the $^3S_1$ partial wave the rank-3 separable potential reproduces quite well the RGM+OCM phase shift. In the other cases the rank-3 separable potential reproduces equally well the RGM+OCM+LS phase shifts.

TABLE X. Parameters $a_{n,m}$ of the form factor of Eq. (4.4) for the $^3S_1$ potential. The first column gives the rank-1 parameters with λ_{11} =-0.25598940$\times 10^1$

$a_{1,m}$	$a_{2,m}$	$a_{3,m}$
0.74418704$\times 10^1$	-0.13197287$\times 10^3$	-0.16817810$\times 10^2$
-0.99634394$\times 10^1$	0.10665018$\times 10^3$	0.11212182$\times 10^2$
0.23859818$\times 10^2$	-0.30740737$\times 10^3$	-0.35992162$\times 10^2$
-0.27331253$\times 10^2$	0.28417959$\times 10^3$	0.28919328$\times 10^2$
0.20995060$\times 10^2$	-0.17596997$\times 10^3$	-0.15737689$\times 10^2$
-0.11699246$\times 10^2$	0.75921030$\times 10^2$	0.56602713$\times 10^1$
0.50516284$\times 10^1$	-0.25132501$\times 10^2$	-0.14815321$\times 10^1$
-0.17466475$\times 10^1$	0.68293763$\times 10^1$	0.30459200
0.48893164	-0.16061242$\times 10^1$	-0.56883879$\times 10^{-1}$
-0.11058936	0.33443137	0.11406159$\times 10^{-1}$
0.20040057$\times 10^{-1}$	-0.60527031$\times 10^{-1}$	-0.23718437$\times 10^{-2}$
-0.28772181$\times 10^{-2}$	0.91323541$\times 10^{-2}$	0.42859938$\times 10^{-3}$
0.32324420$\times 10^{-3}$	-0.11020710$\times 10^{-2}$	-0.60155849$\times 10^{-4}$
-0.28013348$\times 10^{-4}$	0.10296990$\times 10^{-3}$	0.62866235$\times 10^{-5}$
0.18394221$\times 10^{-5}$	-0.72504967$\times 10^{-5}$	-0.47999987$\times 10^{-6}$
-0.89281320$\times 10^{-7}$	0.37402881$\times 10^{-6}$	0.26272042$\times 10^{-7}$
0.30874015$\times 10^{-8}$	-0.13612727$\times 10^{-7}$	-0.99973788$\times 10^{-9}$
-0.71610131$\times 10^{-10}$	0.32922428$\times 10^{-9}$	0.25040321$\times 10^{-10}$
0.99454633$\times 10^{-12}$	-0.47290138$\times 10^{-11}$	-0.37035448$\times 10^{-12}$

-0.62302608$\times 10^{-14}$	$0.30443574\times 10^{-13}$	$0.24485301\times 10^{-14}$

TABLE XI. Coupling constants $\lambda_{ij} = \lambda_{ji}$ for the rank-3 $^3S_1$ potential.

$\lambda_{11} = 0.25332051\times 10^{1}$
$\lambda_{12} =$-0.44177961
$\lambda_{13} = 0.33554529\times 10^{1}$
$\lambda_{22} =$-0.19258003
$\lambda_{23} = 0.11500883\times 10^{1}$
$\lambda_{33} =$-0.67841091$\times 10^{1}$

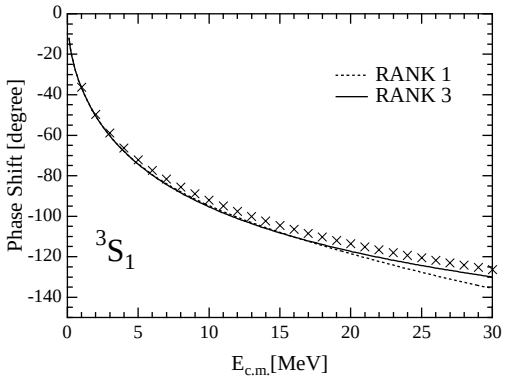

FIG. 9. Phase shifts for the $^3S_1$ partial wave without Coulomb effects. The crosses denote the RGM+OCM result, the dashed line the rank-1 result, and the solid line the rank-3 result, respectively.

TABLE XII. Parameters $a_{n,m}$ of the form factor of Eq. (4.4) for the $^3P_0$ potential. The first column lists the rank-1 parameters with λ_{11} =-0.42316727.

$a_{1,m}$	$a_{2,m}$	$a_{3,m}$
-0.66322212×10^{1}	-0.79077911×10^{1}	-0.59125005×10^{1}
0.10444487×10^{2}	0.55415998×10^{1}	0.24492255×10^{1}
-0.17647766×10^{2}	-0.86712354×10^{1}	-0.38446872×10^{1}
0.16035080×10^{2}	0.44944025×10^{1}	0.77187900
-0.10440381×10^{2}	-0.17971337×10^{1}	0.35090483×10^{-1}
0.52745557×10^{1}	0.78617775	0.12686539
-0.22025734×10^{1}	-0.51578766	-0.30787262
0.77506575	0.31027724	0.24158041
-0.22810778	-0.13698661	-0.11373402
0.54968268×10^{-1}	0.43590322×10^{-1}	0.36741567×10^{-1}
-0.10611771×10^{-1}	-0.10160062×10^{-1}	-0.85776771×10^{-2}
0.16122722×10^{-2}	0.17572875×10^{-2}	0.14804394×10^{-2}
-0.18998460×10^{-3}	-0.22687698×10^{-3}	-0.19056704×10^{-3}
0.17117673×10^{-4}	0.21835886×10^{-4}	0.18287608×10^{-4}
-0.11593237×10^{-5}	-0.15527041×10^{-5}	-0.12969524×10^{-5}
0.57638824×10^{-7}	0.80073563×10^{-7}	0.66726978×10^{-7}
-0.20292626×10^{-8}	-0.28985088×10^{-8}	-0.24102829×10^{-8}
0.47658438×10^{-10}	0.69528124×10^{-10}	0.57703914×10^{-10}
$-0.66681851\times10^{-12}$	$-0.98848850\times10^{-12}$	$-0.81884000\times10^{-12}$
0.41875253×10^{-14}	0.62812081×10^{-14}	0.51931988×10^{-14}

TABLE XIII. Coupling constants $\lambda_{ij} = \lambda_{ji}$ for the rank-3 $^3P_0$ potential.

λ_{11} =-0.32152588$\times 10^2$
λ_{12} = 0.93930066$\times 10^2$
λ_{13} =-0.90374767$\times 10^2$
λ_{22} =-0.29056296$\times 10^3$
λ_{23} = 0.28341791$\times 10^3$
λ_{33} =-0.27758530$\times 10^3$

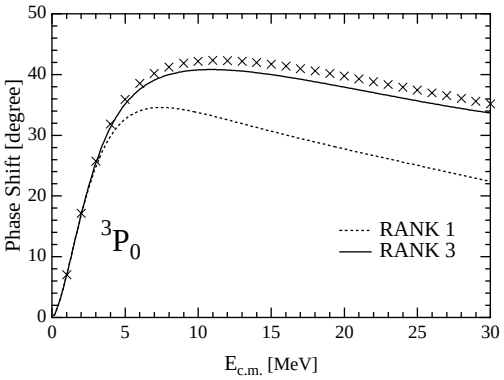

FIG. 10. Phase shifts for the $^3P_0$ state without Coulomb effects. The crosses denote the RGM+OCM+LS result, the dashed line the rank-1 result, and the solid line the rank-3 result, respectively.

TABLE XIV. Parameters $a_{n,m}$ of the form factor of Eq. (4.4) for the $^3P_1$ potential. The first column exhibits the rank-1 parameters with λ_{11} =-0.15329984

$a_{1,m}$	$a_{2,m}$	$a_{3,m}$
-0.11983147×10^2	-0.13550093×10^2	-0.90367514×10^1
0.17014168×10^2	0.73213312×10^1	0.24098258×10^1
-0.28697894×10^2	-0.11569940×10^2	-0.40100766×10^1
0.25268582×10^2	0.43479794×10^1	-0.58369026
-0.16200758×10^2	-0.11052072×10^1	0.96722200
0.81469516×10^1	0.52139426	-0.13854134
-0.34392479×10^1	-0.63361772	-0.38566501
0.12378490×10^1	0.47703657	0.35442445
-0.37446386	-0.22713933	-0.17258809
0.92646826×10^{-1}	0.74443476×10^{-1}	0.56334788×10^{-1}
-0.18290727×10^{-1}	-0.17583617×10^{-1}	-0.13201035×10^{-1}
0.28292359×10^{-2}	0.30615614×10^{-2}	0.22815526×10^{-2}
-0.33808968×10^{-3}	-0.39667201×10^{-3}	-0.29380436×10^{-3}
0.30793834×10^{-4}	0.38250521×10^{-4}	0.28190681×10^{-4}
-0.21030263×10^{-5}	-0.27223565×10^{-5}	-0.19982189×10^{-5}
0.10522448×10^{-6}	0.14041899×10^{-6}	0.10271462×10^{-6}
-0.37222405×10^{-8}	-0.50808201×10^{-8}	-0.37053918×10^{-8}
0.87716868×10^{-10}	0.12175644×10^{-9}	0.88550576×10^{-10}
-0.12300073×10^{-11}	-0.17282223×10^{-11}	-0.12535112×10^{-11}
0.77324366×10^{-14}	0.10955268×10^{-13}	0.79236297×10^{-14}

TABLE XV. Coupling constants $\lambda_{ij} = \lambda_{ji}$ for the rank-3 $^3P_1$ potential.

λ_{11} =-0.10202649$\times 10^2$
λ_{12} = 0.31235498$\times 10^2$
λ_{13} =-0.33737459$\times 10^2$
λ_{22} =-0.10318492$\times 10^3$
λ_{23} = 0.11347250$\times 10^3$
λ_{33} =-0.12541685$\times 10^3$

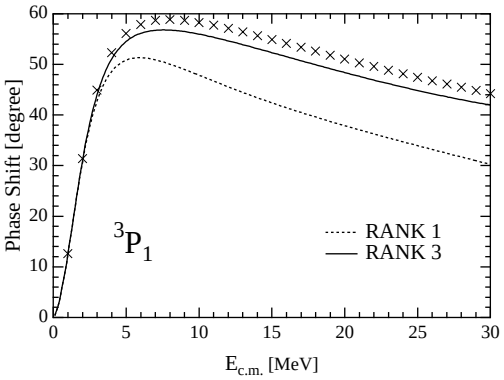

FIG. 11. Phase shifts for the $^3P_1$ partial wave without Coulomb effects. The crosses denote the RGM+OCM+LS result, the dashed line the rank-1 result, and the solid line the rank-3 result, respectively.

TABLE XVI. Parameters $a_{n,m}$ of the form factor of Eq. (4.4) for the $^3P_2$ potential. The first column presents the rank-1 parameters with λ_{11} =-0.66395138$\times 10^{-1}$

$a_{1,m}$	$a_{2,m}$	$a_{3,m}$
-0.18802681$\times 10^{2}$	-0.20111944$\times 10^{2}$	-0.11866155$\times 10^{2}$
0.24695039$\times 10^{2}$	0.86908371$\times 10^{1}$	0.19942254$\times 10^{1}$
-0.41611877$\times 10^{2}$	-0.13903725$\times 10^{2}$	-0.36405995$\times 10^{1}$
0.35688295$\times 10^{2}$	0.31275599$\times 10^{1}$	-0.22992102$\times 10^{1}$
-0.22579637$\times 10^{2}$	0.31524135	0.20651004$\times 10^{1}$
0.11307515$\times 10^{2}$	-0.49795244$\times 10^{-1}$	-0.47700417
-0.48182932$\times 10^{1}$	-0.68502022	-0.42575885
0.17672518$\times 10^{1}$	0.64872070	0.44814211
-0.54652963	-0.32730654	-0.22367571
0.13797319	0.10952640	0.73558687$\times 10^{-1}$
-0.27690659$\times 10^{-1}$	-0.26106999$\times 10^{-1}$	-0.17285137$\times 10^{-1}$
0.43380605$\times 10^{-2}$	0.45661980$\times 10^{-2}$	0.29907200$\times 10^{-2}$
-0.52342569$\times 10^{-3}$	-0.59304311$\times 10^{-3}$	-0.38526921$\times 10^{-3}$
0.48023975$\times 10^{-4}$	0.57258765$\times 10^{-4}$	0.36964876$\times 10^{-4}$
-0.32978152$\times 10^{-5}$	-0.40774761$\times 10^{-5}$	-0.26191716$\times 10^{-5}$
0.16568211$\times 10^{-6}$	0.21032277$\times 10^{-6}$	0.13454055$\times 10^{-6}$
-0.58782654$\times 10^{-8}$	-0.76069363$\times 10^{-8}$	-0.48484250$\times 10^{-8}$
0.13880285$\times 10^{-9}$	0.18213056$\times 10^{-9}$	0.11569505$\times 10^{-9}$
-0.19485870$\times 10^{-11}$	-0.25815323$\times 10^{-11}$	-0.16344262$\times 10^{-11}$
0.12253427$\times 10^{-13}$	0.16330410$\times 10^{-13}$	0.10302405$\times 10^{-13}$

TABLE XVII. Coupling constants $\lambda_{ij} = \lambda_{ji}$ for the rank-3 $^3P_2$ potential.

λ_{11} =-0.41423805×10^1
λ_{12} = 0.13294740×10^2
λ_{13} =-0.16229175×10^2
λ_{22} =-0.46727996×10^2
λ_{23} = 0.58280329×10^2
λ_{33} =-0.73111775×10^2

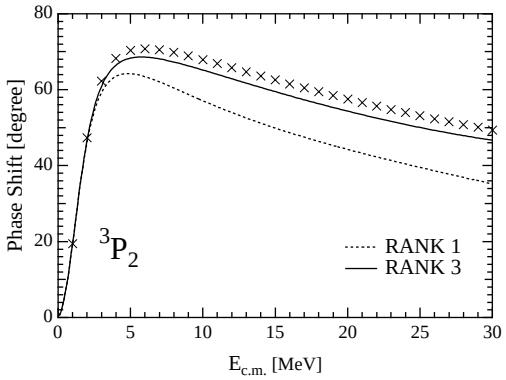

FIG. 12. Phase shifts for $^3P_2$ state without Coulomb effects. The crosses denote the RGM+OCM+LS result, the dashed line the rank-1 result, and the solid line the rank-3 result, respectively.

TABLE XVIII. Parameters $a_{n,m}$ of the form factor of Eq. (4.4) for the $^3D_1$ potential. The first column lists the rank-1 parameters with $\lambda_{11} = 0.38702146\times10^2$.

$a_{1,m}$	$a_{2,m}$	$a_{3,m}$
0.89936516	0.26418769×10^1	0.23149927×10^1
-0.26186344×10^1	-0.76699755×10^1	-0.69187833×10^1
0.40420417×10^1	0.10171559×10^2	0.80438855×10^1
-0.37254532×10^1	-0.77481279×10^1	-0.53201948×10^1
0.24045068×10^1	0.40778272×10^1	0.23638415×10^1
-0.11674331×10^1	-0.15957158×10^1	-0.74115241
0.44371340	0.48775235	0.16543078
-0.13423928	-0.11887084	-0.23546429×10^{-1}
0.32471944×10^{-1}	0.23244826×10^{-1}	0.82565419×10^{-3}
-0.62682883×10^{-2}	-0.36286167×10^{-2}	0.57391815×10^{-3}
0.96078361×10^{-3}	0.44617253×10^{-3}	-0.17882613×10^{-3}
-0.11613293×10^{-3}	-0.42259918×10^{-4}	0.30875386×10^{-4}
0.10972859×10^{-4}	0.29721861×10^{-5}	-0.36884776×10^{-5}
-0.80105503×10^{-6}	-0.14441536×10^{-6}	0.32121255×10^{-6}
0.44458731×10^{-7}	0.39214969×10^{-8}	-0.20613138×10^{-7}
-0.18322050×10^{-8}	0.15747854×10^{-10}	0.96582033×10^{-9}
0.54076554×10^{-10}	$-0.61093792\times10^{-11}$	$-0.32154572\times10^{-10}$
$-0.10765494\times10^{-11}$	0.24518321×10^{-12}	0.72109404×10^{-12}
0.12907316×10^{-13}	$-0.45959801\times10^{-14}$	$-0.97789252\times10^{-14}$
$-0.70194793\times10^{-16}$	0.35260306×10^{-16}	0.60733413×10^{-16}

TABLE XIX. Coupling constants $\lambda_{ij} = \lambda_{ji}$ for the rank-3 $^3D_1$ potential.

λ_{11} =-0.12403227$\times 10^5$
λ_{12} = 0.72374384$\times 10^4$
λ_{13} =-0.33925562$\times 10^4$
λ_{22} =-0.42322025$\times 10^4$
λ_{23} = 0.19982358$\times 10^4$
λ_{33} =-0.95274067$\times 10^3$

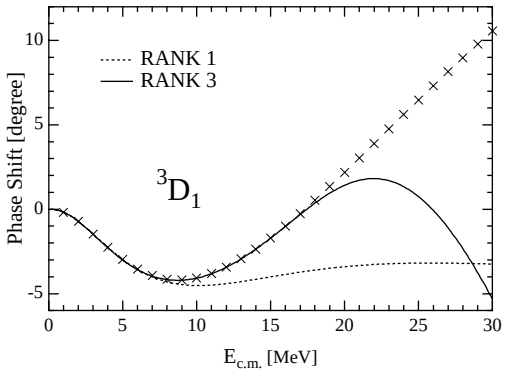

FIG. 13. Phase shifts for $^3D_1$ state without Coulomb effects. The crosses denote the RGM+OCM+LS result, the dashed line the rank-1 result, and the solid line the rank-3 result, respectively.

TABLE XX. Parameters $a_{n,m}$ of the form factor of Eq. (4.4) for the $^3D_2$ potential. The first column exhibits the rank-1 parameters with $\lambda_{11} = 0.59024361\times10^2$

$a_{1,m}$	$a_{2,m}$	$a_{3,m}$
0.57066711	0.16484822×10^1	0.14099209×10^1
-0.16583375×10^1	-0.47749159×10^1	-0.42072799×10^1
0.25409617×10^1	0.62850269×10^1	0.48779676×10^1
-0.23332252×10^1	-0.47697116×10^1	-0.32222764×10^1
0.15018139×10^1	0.25024490×10^1	0.14316862×10^1
-0.72790438	-0.97809048	-0.45159892
0.27639429	0.29955475	0.10332838
-0.83595442×10^{-1}	-0.73538742×10^{-1}	$-0.161848780\times10^{-1}$
0.20227441×10^{-1}	0.14601065×10^{-1}	0.127725469×10^{-2}
-0.39078222×10^{-2}	-0.23406505×10^{-2}	0.124271741×10^{-3}
0.59974333×10^{-3}	0.30037269×10^{-3}	$-0.610339620\times10^{-4}$
-0.72616864×10^{-4}	-0.30435345×10^{-4}	0.111994241×10^{-4}
0.68758985×10^{-5}	0.23895692×10^{-5}	$-0.133580683\times10^{-5}$
-0.50325849×10^{-6}	-0.14163274×10^{-6}	0.113449284×10^{-6}
0.28016277×10^{-7}	0.60927632×10^{-8}	$-0.701058725\times10^{-8}$
-0.11587213×10^{-8}	-0.17749233×10^{-9}	0.313672923×10^{-9}
0.34341671×10^{-10}	0.29770498×10^{-11}	$-0.991409110\times10^{-11}$
$-0.68698690\times10^{-12}$	$-0.11337993\times10^{-13}$	$0.210314951\times10^{-12}$
0.82832450×10^{-14}	$-0.48655006\times10^{-15}$	$-0.269557305\times10^{-14}$
$-0.45347221\times10^{-16}$	0.63794448×10^{-17}	$0.158651456\times10^{-16}$

TABLE XXI. Coupling constants $\lambda_{ij} = \lambda_{ji}$ for the rank-3 $^3D_2$ potential.

$\lambda_{11} = 0.28519285\times10^5$
$\lambda_{12} =$-0.17108157$\times10^5$
$\lambda_{13} = 0.84546586\times10^4$
$\lambda_{22} = 0.10247694\times10^5$
$\lambda_{23} =$-0.50401399$\times10^4$
$\lambda_{33} = 0.24628297\times10^4$

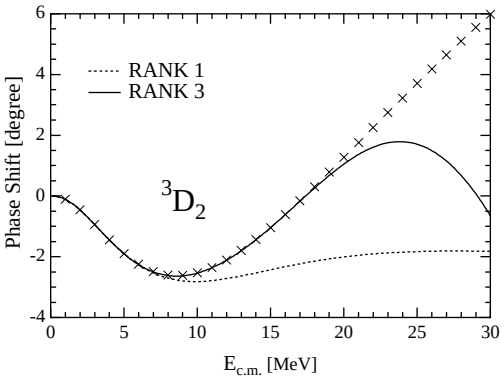

FIG. 14. Phase shifts for $^3D_2$ state without Coulomb effects. The crosses denote the RGM+OCM+LS result, the dashed line the rank-1 result, and the solid line the rank-3 result, respectively.

TABLE XXII. Parameters $a_{n,m}$ of the form factor of Eq. (4.4) for the $^3D_3$ potential. The first column gives the rank-1 parameters with $\lambda_{11} = 0.48683315\times10^2$

$a_{1,m}$	$a_{2,m}$	$a_{3,m}$
0.70053005	0.20372307×10^1	0.17586107×10^1
-0.20371819×10^1	-0.59058643×10^1	-0.52507453×10^1
0.31301669×10^1	0.77955339×10^1	0.60941222×10^1
-0.28784057×10^1	-0.59247131×10^1	-0.40278443×10^1
0.18547114×10^1	0.31124541×10^1	0.17900376×10^1
-0.89957466	-0.12173452×10^1	-0.563742149
0.34172242	0.37272087	0.128054107
-0.10337205	-0.91321241×10^{-1}	$-0.195064865\times10^{-1}$
0.25011910×10^{-1}	0.18051377×10^{-1}	0.129543369×10^{-2}
-0.48311038×10^{-2}	-0.28709573×10^{-2}	0.243205612×10^{-3}
0.74115882×10^{-3}	0.36379018×10^{-3}	$-0.950679435\times10^{-4}$
-0.89691472×10^{-4}	-0.36150992×10^{-4}	0.169973636×10^{-4}
0.84868416×10^{-5}	0.27543762×10^{-5}	$-0.203045225\times10^{-5}$
-0.62064686×10^{-6}	-0.15550511×10^{-6}	0.174498404×10^{-6}
0.34516816×10^{-7}	0.61282950×10^{-8}	$-0.109761505\times10^{-7}$
-0.14259032×10^{-8}	-0.14661306×10^{-9}	0.502037641×10^{-9}
0.42202574×10^{-10}	0.10222286×10^{-11}	$-0.162758205\times10^{-10}$
$-0.84290188\times10^{-12}$	0.50688694×10^{-13}	$0.355038528\times10^{-12}$
0.10144471×10^{-13}	$-0.15433806\times10^{-14}$	$-0.468513806\times10^{-14}$
$-0.55417256\times10^{-16}$	0.14088408×10^{-16}	$0.283746588\times10^{-16}$

TABLE XXIII. Coupling constants $\lambda_{ij} = \lambda_{ji}$ for the rank-3 ^{3}D$_3$ potential.

$\lambda_{11} = 0.17437597\times10^{6}$
$\lambda_{12} =$-0.10347752×10^{6}
$\lambda_{13} = 0.50147622\times10^{5}$
$\lambda_{22} = 0.61393167\times10^{5}$
$\lambda_{23} =$-0.29733363×10^{5}
$\lambda_{33} = 0.14387562\times10^{5}$

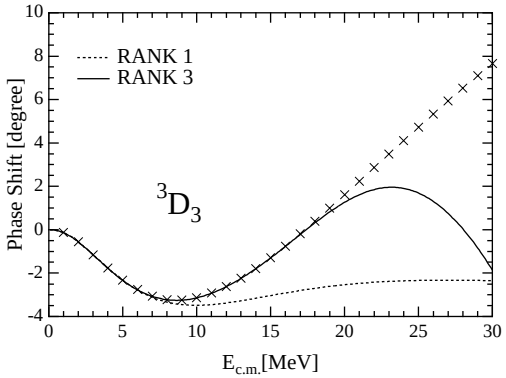

FIG. 15. Phase shifts for $^3D_3$ state without Coulomb effects. The crosses denote the RGM+OCM+LS result, the dashed line the rank-1 result, and the solid line the rank-3 result, respectively.

TABLE XXIV. Parameters $a_{n,m}$ of the form factor of Eq. (4.4) for the $^3F_2$ potential. The first column gives the rank-1 parameters with λ_{11} =-0.15280632$\times 10^4$

$a_{1,m}$	$a_{2,m}$	$a_{3,m}$
-0.10519807	-0.10795104$\times 10^1$	-0.11657860$\times 10^1$
0.26681674	0.22362235$\times 10^1$	0.20871658$\times 10^1$
-0.38458973	-0.29306786$\times 10^1$	-0.25641087$\times 10^1$
0.33899788	0.22258120$\times 10^1$	0.17311373$\times 10^1$
-0.20956819	-0.11544199$\times 10^1$	-0.759879540
0.96873287$\times 10^{-1}$	0.42971181	0.208280611
-0.34663036$\times 10^{-1}$	-0.11609305	-0.224855812$\times 10^{-1}$
0.97602881$\times 10^{-2}$	0.21859658$\times 10^{-1}$	-0.890945285$\times 10^{-2}$
-0.21786339$\times 10^{-2}$	-0.24236811$\times 10^{-2}$	0.551995844$\times 10^{-2}$
0.38647216$\times 10^{-3}$	-0.54141248$\times 10^{-5}$	-0.161738180$\times 10^{-2}$
-0.54465017$\times 10^{-4}$	0.60393519$\times 10^{-4}$	0.316664790$\times 10^{-3}$
0.60817595$\times 10^{-5}$	-0.12963497$\times 10^{-4}$	-0.447135268$\times 10^{-4}$
-0.53523779$\times 10^{-6}$	0.16249029$\times 10^{-5}$	0.466785193$\times 10^{-5}$
0.36794342$\times 10^{-7}$	-0.13891113$\times 10^{-6}$	-0.362189145$\times 10^{-6}$
-0.19476964$\times 10^{-8}$	0.83947022$\times 10^{-8}$	0.207493943$\times 10^{-7}$
0.77622991$\times 10^{-10}$	-0.35813659$\times 10^{-9}$	-0.862103751$\times 10^{-9}$
-0.22468227$\times 10^{-11}$	0.10514171$\times 10^{-10}$	0.251419959$\times 10^{-10}$
0.44459234$\times 10^{-13}$	-0.20104072$\times 10^{-12}$	-0.485787313$\times 10^{-12}$
-0.53628444$\times 10^{-15}$	0.22387162$\times 10^{-14}$	0.556075874$\times 10^{-14}$
0.29648478$\times 10^{-17}$	-0.10924776$\times 10^{-16}$	-0.284419168$\times 10^{-16}$

TABLE XXV. Coupling constants $\lambda_{ij} = \lambda_{ji}$ for the rank-3 $^3\mathrm{F}_2$ potential.

λ_{11} =-0.22056858$\times 10^6$
λ_{12} = 0.53156082$\times 10^5$
λ_{13} =-0.29476815$\times 10^5$
λ_{22} =-0.13088707$\times 10^5$
λ_{23} = 0.73245374$\times 10^4$
λ_{33} =-0.41218725$\times 10^4$

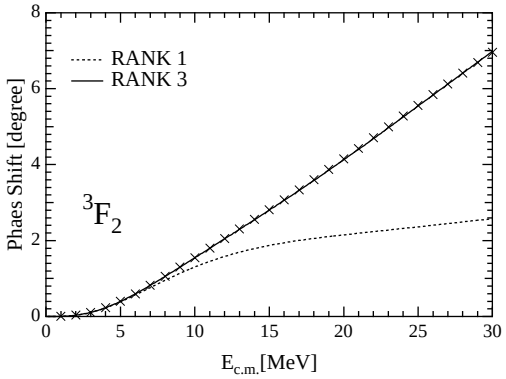

FIG. 16. Phase shifts for $^3F_2$ state without Coulomb effects. The crosses denote the RGM+OCM+LS result, the dashed line the rank-1 result, and the solid line the rank-3 result, respectively.

TABLE XXVI. Parameters $a_{n,m}$ of the form factor of Eq. (4.4) for the $^3F_3$ potential. The first column lists the rank-1 parameters with λ_{11} =-0.15533123$\times 10^4$

$a_{1,m}$	$a_{2,m}$	$a_{3,m}$
-0.10355351	-0.10619702$\times 10^1$	-0.11465411$\times 10^1$
0.26271214	0.22009693$\times 10^1$	0.20540811$\times 10^1$
-0.37869541	-0.28848496$\times 10^1$	-0.25239699$\times 10^1$
0.33382672	0.21914494$\times 10^1$	0.17046664$\times 10^1$
-0.20638383	-0.11368554$\times 10^1$	-0.748665750
0.95407758$\times 10^{-1}$	0.42333402	0.205500714
-0.34141350$\times 10^{-1}$	-0.11445199	-0.223823711$\times 10^{-1}$
0.96143050$\times 10^{-2}$	0.21585398$\times 10^{-1}$	-0.867190389$\times 10^{-2}$
-0.21462844$\times 10^{-2}$	-0.24058411$\times 10^{-2}$	0.540397503$\times 10^{-2}$
0.38078040$\times 10^{-3}$	-0.75437723$\times 10^{-6}$	-0.158522915$\times 10^{-2}$
-0.53669961$\times 10^{-4}$	0.58646658$\times 10^{-4}$	0.310495776$\times 10^{-3}$
0.59937965$\times 10^{-5}$	-0.12652563$\times 10^{-4}$	-0.438486050$\times 10^{-4}$
-0.52756756$\times 10^{-6}$	0.15883035$\times 10^{-5}$	0.457758155$\times 10^{-5}$
0.36271728$\times 10^{-7}$	-0.13585744$\times 10^{-6}$	-0.355154343$\times 10^{-6}$
-0.19202569$\times 10^{-8}$	0.82111556$\times 10^{-8}$	0.203430516$\times 10^{-7}$
0.76537251$\times 10^{-10}$	-0.35024827$\times 10^{-9}$	-0.845015123$\times 10^{-9}$
-0.22155859$\times 10^{-11}$	0.10278242$\times 10^{-10}$	0.246353323$\times 10^{-10}$
0.43844231$\times 10^{-13}$	-0.19638883$\times 10^{-12}$	-0.475781212$\times 10^{-12}$
-0.52889751$\times 10^{-15}$	0.21844895$\times 10^{-14}$	0.544288742$\times 10^{-14}$
0.29241713$\times 10^{-17}$	-0.10642051$\times 10^{-16}$	-0.278159322$\times 10^{-16}$

TABLE XXVII. The coupling constants $\lambda_{ij} = \lambda_{ji}$ for the rank-3 $^3\mathrm{F}_3$ potential.

λ_{11} =-0.22415203$\times 10^6$
λ_{12} = 0.54047498$\times 10^5$
λ_{13} =-0.29976913$\times 10^5$
λ_{22} =-0.13315252$\times 10^5$
λ_{23} = 0.74528575$\times 10^4$
λ_{33} =-0.41950064$\times 10^4$

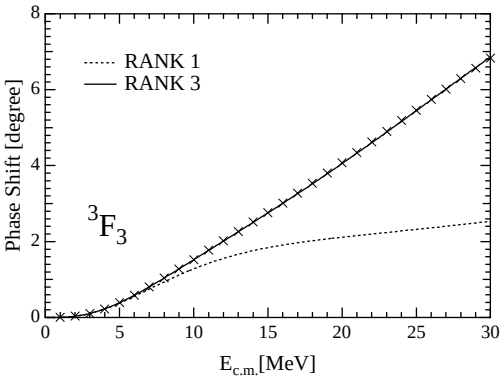

FIG. 17. Phase shifts for $^3F_2$ state without Coulomb effects. The crosses denote the RGM+OCM+LS result, the dashed line the rank-1 result, and the solid line the rank-3 result, respectively.

TABLE XXVIII. Parameters $a_{n,m}$ of the form factor of Eq. (4.4) for the $^3F_4$ potential. The first column exhibits the rank-1 parameters with $^3F_4$ λ_{11} =-0.12982093×10^4

$a_{1,m}$	$a_{2,m}$	$a_{3,m}$
-0.12296582	-0.12705383×10^1	-0.13761116×10^1
0.31102049	0.26178431×10^1	0.24457908×10^1
-0.44801941	-0.34259243×10^1	-0.29980301×10^1
0.39459099	0.25961039×10^1	0.20157805×10^1
-0.24377244	-0.13430375×10^1	-0.87938384
0.11259879	0.49776587	0.23706582
-0.40253696×10^{-1}	-0.13336950	-0.22922059×10^{-1}
0.11322223×10^{-1}	0.24641103×10^{-1}	-0.11752433×10^{-1}
-0.25240891×10^{-2}	-0.25611382×10^{-2}	0.68583670×10^{-2}
0.44711789×10^{-3}	-0.68617181×10^{-4}	-0.19848209×10^{-2}
-0.62915174×10^{-4}	0.81559745×10^{-4}	0.38692325×10^{-3}
0.70141424×10^{-5}	-0.16636723×10^{-4}	-0.54555554×10^{-4}
-0.61631030×10^{-6}	0.20532442×10^{-5}	0.56956135×10^{-5}
0.42302672×10^{-7}	-0.17453341×10^{-6}	-0.44240794×10^{-6}
-0.22361094×10^{-8}	0.10535983×10^{-7}	0.25394314×10^{-7}
0.89005384×10^{-10}	-0.45039190×10^{-9}	-0.10580995×10^{-8}
-0.25735098×10^{-11}	0.13286312×10^{-10}	0.30978486×10^{-10}
0.50877050×10^{-13}	-0.25608145×10^{-12}	-0.60169351×10^{-12}
-0.61321127×10^{-15}	0.28865188×10^{-14}	0.69356947×10^{-14}
0.33875686×10^{-17}	-0.14345838×10^{-16}	-0.35807821×10^{-16}

TABLE XXIX. Coupling constants $\lambda_{ij} = \lambda_{ji}$ for the rank-3 $^3\mathrm{F}_4$ potential.

λ_{11} =-0.18792638$\times 10^6$
λ_{12} = 0.45033170$\times 10^5$
λ_{13} =-0.24918509$\times 10^5$
λ_{22} =-0.11024146$\times 10^5$
λ_{23} = 0.61549429$\times 10^4$
λ_{33} =-0.34552195$\times 10^4$

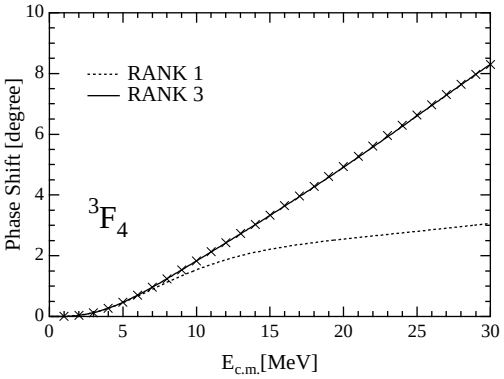

FIG. 18. Phase shifts for $^3F_4$ state without Coulomb effects. The crosses denote the RGM+OCM+LS result, the dashed line the rank-1 result, and the solid line the rank-3 result, respectively.

In the higher energy region (above the break up threshold for ^{3}He→d+p), absorption effects stemming from inelasticity should be considered. This requires the introduction of an imaginary component in the potential. We modified our potential to reproduce the reflection parameters, given by Yoshino *et al.* [19] at E_{Lab}=19.48 MeV, using the anzatz

$$V^{\mathrm{C(LS)}} = \{AC_0 + A^*[C_1(\boldsymbol{L}\cdot\boldsymbol{S}) + C_2(\boldsymbol{L}\cdot\boldsymbol{S})^2 + C_3(\boldsymbol{L}\cdot\boldsymbol{S})^3]\}V^{\mathrm{MOCM}}, \tag{4.6}$$

where the parameters C_0, C_1, C_2, C_3 are the same as in the $V^{\mathrm{OCM(LS)}}$ potential. And the complex factor A is chosen as follows

$$A = 1 + ia\{1 - e^{-bE_{th}^2}\}\theta(E_{th}) \tag{4.7}$$

where A^* is the complex conjugate of A, and a=21.0, b=2.50×10^{-5}, respectively. The break up threshold energy E_{th} is given by $E_{th} = E - E_h + E_d$, E_h and E_d are the ^{3}He and the deuteron binding energies respectively, while $\theta(x)$ is the step function. Using this complex potential, we calculated the phase shifts and found that they change, at most, by a few degrees in the region of 19.48 MeV. Therefore, we do not present these results in this paper.

V. DISCUSSION AND CONCLUSIONS

We constructed the p-^{3}He effective potentials up to L=3 based on the RGM combined with the OCM technique which removes the PFS. These models do not include either an LS or a tensor force, which were not included in the nucleon-nucleon potential used to construct the nucleon-trinucleon potential. In the present work, we introduce the LS interaction phenomenologically at an intercluster level. This successfully describes the degeneracy in the spin–triplet (^{3}P$_0$,^{3}P$_1$, ^{3}P$_2$), (^{3}D$_1$, ^{3}D$_2$,^{3}D$_3$), and (^{3}F$_2$, ^{3}F$_3$,^{3}F$_4$) channels. The tensor force could be similarly included. However, these forces could be safely omitted as their influence on the data was shown, in the recent work of Yoshino *et al.* [19], to be very small.

In the higher energy region (above the break up threshold), absorption effects can be included via Eq. (4.6). Since, however, our main concern is the construction of potentials at low energies, little attention was given to the construction of complex potential (see forth Eq. (4.7)).

The theoretical (RGM) phase shifts are well reproduced by our potentials. As far as the experimental phase shifts are concerned, it should be noted that the results obtained by various analyses are not in agreement to each other. However, our potentials fit the most recent phase shifts [19] quite well. Furthermore, we compared our results with those of Ref. [10], which are based on a Yamaguchi type separable potential fitted to lower energy scattering data. The latter potentials reproduce well the differential cross sections at very low energies.

Special attention was paid to effects of non-central forces in each of the negative parity states, 2^-, 1^-, 0^-. We derived the energy spectrum by using the phase-shift data by Beltramin *et al.* (BFP) Ref. [10] employing the three-dimensional Spline function interpolation method. Our result is compared with the BFP spectrum and with the GCM calculation Ref. [21] as well as with the experimental data. The results are plotted in Fig. 19. The first and the second lowest levels of the BFP crossed each other. The GCM calculation reproduces the ordering of four negative parity states but the spectrum is totally shifted to a higher energy region, while our results are in good agreement with the experimental data in which the lowest level 2^- is due to the $^3P_2$ state, the second lowest 1^- level to $^3P_1$, the 0^- level to $^3P_0$, and the excited 1^- level to the $^1P_1$ state.

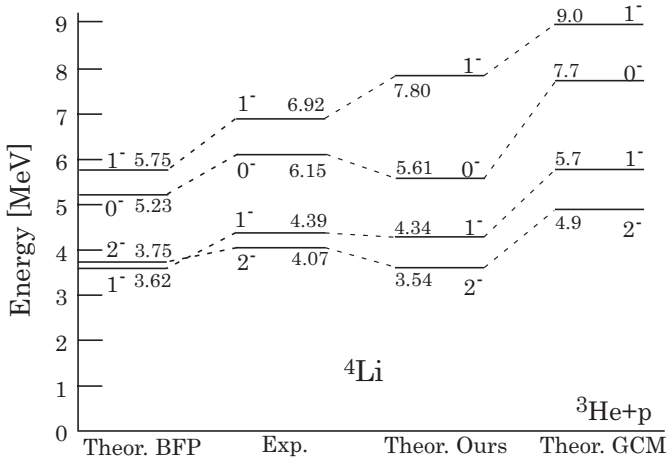

FIG. 19. ^{4}Li resonance energy level above the p–^{3}He threshold. The experimental data are taken from Ref. [22], Theor. BFP are the results of Ref. [10], Theor. GCM by Ref. [21], and Theor. Ours are the results of the present work.

From the overall results, we may conclude that our potentials (RGM+OCM plus phenomenological LS force) reproduce the scattering and resonance state data of the p-^{3}He system well. Concerning the OCM results, we note that they are essentially on-shell equivalent to the RGM one. However, we found that there are some differences, albeit small, in the phase shift for the P and D waves.

Finally, our EST separable potentials can be used in few-cluster systems where p-^{3}He is involved. One such reaction is ^{3}He(d,p)^{4}He, which can be treated as a three-body system, p-n-^{3}He, within the Faddeev integral equations. Moreover, they can be used for interpretation purposes by constructing local equivalent interactions which can provide us a further insight into the interaction between light clusters, their characteristics concerning shape, range *etc.*, as well as their bound and resonance structure. The understanding of the interaction

between light clusters will pave the way for a better treatment of few-cluster systems and their role in nuclear reactions and primordial nucleosynthesis.

ACKNOWLEDGMENTS

The authors wish to thank H. Kamada, S. Nakamura, K. Samata, and T.Yamada for valuable discussions and technical supports. This work was done using the computers in *FRCCS* of Science University of Tokyo, *RIKEN*, National Astronomical Observatory of Japan, and National Institute for Fusion Science.

APPENDIX A: RESONATING GROUP METHOD AND THE ORTHOGONALITY CONDITION MODEL

In what follows we outline for convenience the RGM for the p-^{3}He system. The total wave function for the p-^{3}He system is defined by

$$\Psi = \mathcal{A}[\phi_{\rm CL}\,\xi(\sigma,\tau)\,\chi(\boldsymbol{R}_N - \boldsymbol{R}_{\rm CL})], \tag{A1}$$

where $\mathcal{A}$ is the antisymmetrization operator, $\xi(\sigma,\tau)$ the isospin function, and $\chi(\boldsymbol{R}_N - \boldsymbol{R}_{\rm CL})$ the relative wave function between the clusters, while $\phi_{\rm CL}$ is the internal wave function of the clusters which is defined by superimposing two Gaussian functions

$$\begin{aligned}\phi_{\rm CL} = &\exp[-\frac{1}{2}\alpha_1 \sum_{i=1}^{3}(\boldsymbol{r}_i - \boldsymbol{R}_{\rm CL})^2] \\ &+ c\exp[-\frac{1}{2}\alpha_2 \sum_{i=1}^{3}(\boldsymbol{r}_i - \boldsymbol{R}_{\rm CL})^2].\end{aligned} \tag{A2}$$

Here $\boldsymbol{R}_{\rm CL}$ is the center of mass of the ^{3}He cluster and $\boldsymbol{r}_i$ are the coordinates of nucleons within the ^{3}He cluster. The parameters α_1, α_2, and c are taken from Ref. [20], namely, $\alpha_1 = 0.25$ fm^{-2}, $\alpha_2 = 0.71$ fm^{-2}, and $c = 3.17$. The Hamiltonian is given by

$$H = H_0 + \sum_{i>j} V_{ij}, \tag{A3}$$

where H_0 is the total kinetic energy and V_{ij} are the interactions between the (i,j) nucleons. The relative function $\chi(\boldsymbol{R}_N - \boldsymbol{R}_{\rm CL})$ can be evaluated variationally by considering

$$\langle \delta\Psi | H - E' | \Psi \rangle = 0, \tag{A4}$$

where E' is the total energy of the whole system. In this model, the total energy is separated into the internal energy of the cluster E_{int} and the relative energy between the colliding clusters E, *i.e.* $E' = E + E_{int}$. Using Eq. (A2) in Eq. (A4) one can obtain the following integro-differential equation,

$$\left(\frac{\hbar^2}{2\mu}\nabla^2_{\boldsymbol{r}} - V_D(\boldsymbol{r}) + E\right)\chi(\boldsymbol{r}) = \int_0^\infty K(\boldsymbol{r},\boldsymbol{r}')\chi(\boldsymbol{r}')\,{\rm d}\boldsymbol{r}', \tag{A5}$$

where V_D is the Direct local potential and $K(\mathbf{r},\mathbf{r}')$ is the corresponding nonlocal one which consists of three terms

$$K(\boldsymbol{r},\boldsymbol{r}') = K_T(\boldsymbol{r},\boldsymbol{r}') + K_V(\boldsymbol{r},\boldsymbol{r}') + E'\mathcal{N}(\boldsymbol{r},\boldsymbol{r}'), \tag{A6}$$

where K_T is obtained from the kinetic energy term, K_V from the potential term, and $\mathcal{N}$ is often referred to as the norm-integral kernel or the norm kernel. In operator form Eq. (A5) is written as

$$(h_0 + V_D + K_T + K_V + E'\mathcal{N})\chi = E\chi \tag{A7}$$

where E and h_0 are the relative energy and the kinetic operator between the ^{3}He cluster and the proton, respectively. The RGM (effective) potential can be identified to

$$V^{\rm RGM}(E) \equiv V_D + K_T + K_V + E'\mathcal{N} = W + E\mathcal{N} \tag{A8}$$

with

$$W = V_D + K_T + K_V + E_{int}\mathcal{N}. \tag{A9}$$

The normalization of the total wave function of the system is given by

$$1 = \langle\Psi|\Psi\rangle = \langle\phi_a\phi_b\chi|\mathcal{A}[\phi_a\phi_b\chi]\rangle = \langle\chi|(1-\mathcal{N})|\chi\rangle \equiv \langle\psi|\psi\rangle, \tag{A10}$$

where ϕ_a is the ^{3}He cluster intrinsic wave function while ϕ_b is a single nucleon wave function. It is, however, known that the norm of the relative function χ is not one and therefore one defines the function ψ,

$$\psi = \sqrt{1-\mathcal{N}}\,\chi\,, \tag{A11}$$

which has the proper probability density interpretation as the physical wave function.

An additional problem with the RGM formalism is the existence of PFS. These states can be removed using the OCM technique in which Eq. (A7) is rewritten as follows,

$$(h_0 + V_D + K_T + K_V + E_{int}\mathcal{N})\chi = E(1-\mathcal{N})\chi. \tag{A12}$$

Furthermore, using Eq. (A11) one obtains

$$\frac{1}{\sqrt{1-\mathcal{N}}}(h_0 + V_D + K_T + K_V + E_{int}\mathcal{N})\frac{1}{\sqrt{1-\mathcal{N}}}\psi = E\psi. \tag{A13}$$

Therefore, the Pauli corrected intercluster potential is

$$V^{\rm OCM} = \frac{1}{\sqrt{1-\mathcal{N}}}\,(\,h_0 + V_D + K_T + K_V + E_{int}\mathcal{N}\,)\,\frac{1}{\sqrt{1-\mathcal{N}}} - h_0\,. \tag{A14}$$

A Pauli forbidden state is removed when the corresponding eigen-value of $\sqrt{1-\mathcal{N}}$ vanishes. It should be noted that in this representation the energy dependence of the potential is eliminated.

The potential $V^{\rm OCM}$ in Eq. (A14) is given in operator form. It can, however, be easily brought into a more suitable form for numerical calculation. For this, when the cluster wave function is given by one Gaussian term, the eigen-function of the norm kernel $\mathcal{N}$ is found using the harmonic oscillator function [26]. In the present case, however, where the ^{3}He wave function is given by two Gaussian terms, the norm eigen-function is a superposition of harmonic oscillator functions. Now, the norm kernel $\mathcal{N}$ is given by

$$\mathcal{N} = \sum_{ij=1}^{\infty} |U_i\rangle G_{ij} \langle U_j| \tag{A15}$$

where

$$G_{ij} \equiv \langle U_i|\mathcal{N}|U_j\rangle. \tag{A16}$$

The matrix elements of the norm kernel analytically while the matrix can be diagonalized numerically using the Jacobo method. For this, Eq. (A15) is written as

$$\begin{aligned}\mathcal{N} &= \sum_{ijk=1}^{\infty} |U_i\rangle a_{ik}\gamma_k a^*_{kj}\langle U_j| \\ &= \sum_{k=1}^{\infty} |\tilde{U}_k\rangle \gamma_k \langle \tilde{U}_k| \end{aligned} \tag{A17}$$

where

$$|\tilde{U}_k\rangle \equiv \sum_{i=1}^{\infty} |U_i\rangle a_{ik}\,. \tag{A18}$$

Furthermore, the term γ_k is the eigen-value of the norm kernel and $\tilde{U}_k$ is the corresponding eigen-function. Eq. (A14) then becomes

$$V^{\rm OCM} = \sum_{ij=1}^{\infty} |\tilde{U}_i\rangle [\frac{1}{\sqrt{1-\gamma_i}}(h_{0ij}+W_{ij})\frac{1}{\sqrt{1-\gamma_j}} - h_{0ij}]\langle \tilde{U}_j| \tag{A19}$$

where

$$h_{0ij} \equiv \langle \tilde{U}_i|h_0|\tilde{U}_j\rangle\,, \tag{A20}$$

$$W_{ij} \equiv \langle \tilde{U}_i|W|\tilde{U}_j\rangle\,. \tag{A21}$$

APPENDIX B: MOMENTUM REPRESENTATION

In what follows we also present the above potential in momentum space suitable for the Alt-Grassberger-Sandhas (AGS) equations [33]. The momentum representation is introduced using the Fourier transforms,

$$\mathcal{F}\{f^{(0)}_\ell\} = 4\pi \int_0^\infty f^{(0)}_\ell \cdot j_\ell(kr)\cdot j_\ell(k'r) r^2\,{\rm d}r\,, \tag{B1}$$

$$\mathcal{F}\{f^{(n)}_\ell\} = 4\pi \int_0^\infty f^{(n)}_\ell \cdot j_\ell(kr)\cdot j_\ell(k'r')\,{\rm d}r\,{\rm d}r'\,. \tag{B2}$$

The potential consist of the following set of functions [20].

$$f_\ell^{(0)}(a;r) = \exp(-ar^2) \tag{B3}$$

$$f_\ell^{(1)}(a,a':r,r') = (-i)^\ell rr' \exp(-ar^2 - a'r'^2) j_\ell(ibrr') \tag{B4}$$

$$f_\ell^{(2)}(a,b:r,r') = (-i)^\ell rr'(r^2+r'^2) \exp(-ar^2 - ar'^2) j_\ell(ibrr') \tag{B5}$$

$$f_\ell^{(3)}(a,b:r,r') = (-i)^\ell rr' \exp(-ar^2 - ar'^2)\{(ibrr') j_{L+1}(ibrr') - L \cdot j_\ell(ibrr')\} \tag{B6}$$

$$f_\ell^{(4)}(a,a':r,r') = rr' \exp(-ar^2 - a'r'^2) \tag{B7}$$

$$f_\ell^{(5)}(a:r,r') = rr'(r^2+r'^2) \exp(-ar^2 - ar'^2) \tag{B8}$$

$$f_\ell^{(6)}(a,a',b,c,c':r,r') = (-i)^\ell rr'(cr^2+c'r'^2) \exp(-ar^2 - a'r'^2) j_\ell(ibrr') \tag{B9}$$

$$f_\ell^{(7)}(a,a',b:r,r') = -brr' \exp(-ar^2 - a'r'^2)\{i^{L+1} rr' j_{L+1}(-ibrr') + i^\ell \frac{L}{b} j_\ell(-ibrr')\} \tag{B10}$$

Using the definitions (B1) and (B2) we obtain

$$\mathcal{F}\{f_\ell^{(0)}\} = (-1)^\ell (\frac{\pi}{a})^{3/2} \frac{2a}{kk'} \exp(-\frac{k^2+k'^2}{4a}) \mathcal{J}_{L+1/2}(\frac{kk'}{2a}) \tag{B11}$$

$$\mathcal{F}\{f_\ell^{(1)}\} = 2\pi^2 \frac{-1}{\sqrt{4aa'-b^2}} \frac{1}{bkk'} \exp(-\frac{a'k^2+ak'^2}{4aa'-b^2}) \mathcal{J}_{L+1/2}(-\frac{bkk'}{4aa'-b^2}) \tag{B12}$$

$$\begin{aligned}\mathcal{F}\{f_\ell^{(2)}\} &= \frac{8abkk'}{(4a^2-b^2)^2} \mathcal{I}_{L+1}(a,a,b:k,k') \\ &+ [\frac{4a(2L+3)}{4a^2-b^2} - \frac{(4a^2+b^2)(k^2+k'^2)}{(4a^2-b^2)^2}] \mathcal{I}_\ell(a,a,b:k,k')\end{aligned} \tag{B13}$$

$$\begin{aligned}\mathcal{F}\{f_\ell^{(3)}\} &= -[L + \frac{(2L+3)b^2}{4a^2-b^2} - \frac{2ab^2(k^2+k'^2)}{4a^2-b^2)^2}] \mathcal{I}_\ell(a,a,b:k,k') \\ &- \frac{(4a^2+b^2)bkk'}{(4a^2-b^2)^2} \mathcal{I}_{L+1}(a,a,b:k,k')\end{aligned} \tag{B14}$$

$$\mathcal{F}\{f_\ell^{(4)}\} = \frac{\pi^2}{4} (\frac{1}{aa'})^{3/2} \exp(-\frac{a'k^2+ak'^2}{4aa'}) \tag{B15}$$

$$\mathcal{F}\{f_\ell^{(5)}\} = \frac{\pi^2}{4a^4} [3 - \frac{(k^2+k'^2)}{4a}] \exp(-\frac{k^2+k'^2}{4a}) \tag{B16}$$

$$\begin{aligned}\mathcal{F}\{f_\ell^{(6)}\} &= [c\{\frac{4a(L+3/2)}{4aa'-b^2} - \frac{4a'^2k^2+b^2k'^2}{(4aa'-b^2)^2}\} + c'\{\frac{4a(L+3/2)}{4aa'-b^2} - \frac{4a^2k'^2+b^2k^2}{(4aa'-b^2)^2}\}] \mathcal{I}_\ell(a,a',b:k,k') \\ &+ \frac{4bkk'(a'c+ac')}{(4aa'-b^2)^2} \mathcal{I}_{L+1}(a,a',b:k,k')\end{aligned} \tag{B17}$$

$$\mathcal{F}\{f_\ell^{(7)}\} = \{\frac{2b(L+3/2)}{4aa'-b^2} + \frac{L}{b} - \frac{2b(a'k^2+ak'^2)}{(4aa'-b^2)^2}\} \mathcal{I}_\ell(a,a',b:k,k') + \frac{kk'(4aa'+b^2)}{(4aa'-b^2)^2} \mathcal{I}_{L+1}(a,a',b:k,k')\,. \tag{B18}$$

In the above

$$\mathcal{I}_\ell(a,a',b:k,k') \equiv \mathcal{F}\{f_\ell^{(1)}\} \tag{B19}$$

while $\mathcal{J}_\ell$ is the Hyperbolic Spherical Bessel Function related to the Spherical Bessel Function j_ℓ by

$$\mathcal{J}_{\ell+1/2}(x) = i^\ell\, x\, j_\ell(ix)\,. \tag{B20}$$

REFERENCES

[1] T. Uesaka *et al.*, Phys. Lett. **B421**, 22 (1997); T. Uesaka *et al.*. Nucl. Phys. **A684**, 606c (2001).

[2] S. Oryu, S. Gojuki, T. Hino, E. Uzu, and H. Kamada, Few-Body Systems Suppl. **10**, 371 (1999).

[3] S. Gojuki, H. Kamada, E. Uzu, and S. Oryu, Few-Body Systems Suppl. **12**, 501 (2000).

[4] S. Gojuki, S. Nemoto, S. Oryu, E. Uzu, and H. Kamada, Nucl. Phys. **A684** , 629c (2001).

[5] B. S. Podmore and H. S. Sherif, in *Few-Body Problems and Particle Physics*, ed. by R. J. Slobodrian *et al.* (Laval Univ. Press, Quebec City, Canada, 1995) p 517; H. S. Sherif and B. S. Podmore, in *Few Particle Problems in the Nuclear Interaction*, Ed. I. Slaus *et al.*, (North-Holland publ, 1972) p. 691; H. S. Sherif, Phys. Rev **C19**, 1649 (1979).

[6] V. G. Neudachin, A. A. Sakharuk, and Yu. F. Smirnov, Sov. J. Part. Nucl. **23**, 210 (1992) (Fiz. Elem. Chastits **23**, 479 (1992).

[7] W. T. H. van Oers *et al.*, Phys. Rev. C **65**, 390 (1982).

[8] R. Sciavilla, Phys. Rev. Lett. **65**, 835 (1990).

[9] H. Fiedeldey, S. A. Sofianos, and G. Ellerkmann, Few-Body Systems **18**, 173 (1995).

[10] L. Beltramin, R. del Frate, and G. Pisent, Nucl. Phys. **A442**, 266 (1985).

[11] T. A. Tombrello, C. M. Jones, G. C. Phillips, and J. L. Weil, Nucl. Phys. **39**, 541 (1962).

[12] T. A. Tombrello, Phys. Rev. **138**, B40 (1965).

[13] L. Drigo and G. Pisent, Nuovo Cimento **51**, 419 (1967).

[14] D. H. Mc Sherry and S. D. Baker, Phys. Rev. **C1**, 888 (1970).

[15] R. Darves-Blanc, N. van Sen, J. Arvieux, and J. C. Gondrand, Nucl. Phys. **A191**, 353 (1972)

[16] J. R. Morales, T. A. Cahill, and D. J. Shadoan, Phys. Rev. **C11**, 1905 (1975).

[17] D. Müller, R. Beckmann, and U. Holm, Nucl. Phys. **A311**, 1 (1978).

[18] H. Berg, W. Arnold, E. Huttel, H. H. Krause, J. Ulbricht, and G. Clausnitzer, Nucl. Phys. **A334**, 21 (1980).

[19] Y. Yoshino, V. Limkaisang, J. Nagata, H. Yoshino, and M. Matsuda, Prog. Theor. Phys. **103**, 107 (2000).

[20] I. Reichstein, D. R. Thompson, and Y. C. Tang, Phys. Rev. **C3**, 2139 (1971).

[21] H. Furutani, H. Horiuchi, and R. Tamagaki, Prog. Theor. Phys. **62**, 981 (1979)

[22] D. R. Tilley,H. R. Weller, and G. M. Hale, Nucl. Phys. **A541**, 1 (1992).

[23] M. Teshigawara, K. Katō, and G. F. Filippov, Prog. Theor. Phys, **92**, 79 (1994); M. Teshigawara, K. Katō, and G. F. Filippov private communication.

[24] K. Wildermuth and Y. C. Tang, *A Unified Theory of the Nucleus* (Vieweg, Braunschweig, 1977).

[25] S. Saito, Prog. Theor. Phys. **40**, 893 (1968); S. Saito, Prog. Theor. Phys. **41**, 705 (1969).

[26] S. Oryu, K. Samata, T. Suzuki, S. Nakamura, and H. Kamada, Few Body Systems **17**, 185 (1994).

[27] L. C. McIntyre and W. Haeberli, Nucl. Phys. **A91**, 382 (1967).

[28] D. J. Ernst, C. M. Shakin, and R. M. Thaler, Phys. Rev. **C8**, 46 (1973).

[29] P. Heiss and H. H. Hackenbroich, Nucl. Phys. **A182**, 522 (1972)

[30] S. Oryu, M. Araki, S. Satoh, Prog. Theor, Phys. Suppl. **61**, 199 (1977).

[31] S. Oryu, Phys. Rev. **C27**, 2500 (1983).

[32] V. G. Gorshkov, Soviet Phys. JETP **13**, 1037 (1961); M. L. Goldberger and K. M. Watson, "Collision Theory" John Wiley and Sons, Inc. New York, London, Sydney 1964; E. O. Alt, W. Sandhas and H. Ziegelmann, Phys. Rev. **C17**,1981 (1978).
[33] P. Grassberger and W. Sandhas, Nucl. Phys. **B2**, 181 (1967); E. O. Alt, P. Grassberger, and W. Sandhas, Nucl. Phys. **B2**, 167 (1967).